BRAIN RESEARCH 1135 (2007) 195–200

available at www.sciencedirect.com

ScienceDirect

www.elsevier.com/locate/brainres

BRAIN RESEARCH

Research Report

Expression of S100 protein and protective effect of arundic acid on the rat brain in chronic cerebral hypoperfusion

Ryo Ohtani, Hidekazu Tomimoto , Hideaki Wakita, Hiroshi Kitaguchi, Kayoko Nakaji, Ryosuke Takahashi

Department of Neurology, Kyoto University Graduate School of Medicine, Shogoin, Sakyo-ku, Kyoto 606-8507, Japan

ARTICLE INFO

Article history:
Accepted 30 November 2006
Available online 8 January 2007

Keywords:
White matter
Chronic cerebral hypoperfusion
Apoptosis
Astroglia
S100 protein
Arundic acid

ABSTRACT

S100 protein is expressed primarily by astroglia in the brain, and accumulates in and around the ischemic lesions. Arundic acid, a novel astroglia-modulating agent, is neuroprotective in acute cerebral infarction, whereas the protective effects remain unknown during chronic cerebral hypoperfusion. Rats undergoing chronic cerebral hypoperfusion were subjected to a bilateral ligation of the common carotid arteries, and were allowed to survive for 3, 7 and 14 days. The animals received a daily intraperitoneal injection of 5.0, 10.0 or 20.0 mg/kg of arundic acid, or vehicle, for 14 days. Alternatively, other groups of rats received a delayed intraperitoneal injection of 20.0 mg/kg of arundic acid or vehicle, which started from 1, 3 or 7 days after ligation and continued to 14 days. The degree of white matter (WM) lesions and the numerical density of S100 protein-immunoreactive astroglia were estimated. In the WM of rats with vehicle injections, the number of S100 protein-immunoreactive astroglia increased significantly after chronic cerebral hypoperfusion as compared to the sham-operation. A dosage of 10.0 and 20.0 mg/kg of arundic acid suppressed the numerical increase in S100 protein-immunoreactive astroglia and the WM lesions. These pathological changes were suppressed with delayed treatment up to 7 days in terms of astroglial activation, and up to 3 days in terms of the WM lesions. The protective effects of arundic acid against WM lesions were demonstrated in a dose-dependent manner, and even after postischemic treatments. These results suggest the potential usefulness of arundic acid in the treatment of cerebrovascular WM lesions.

1. Introduction

Ischemic white matter (WM) lesions are frequently observed in human cerebrovascular diseases (CVD), and are believed to be responsible for cognitive impairments in the elderly. It is believed that the occlusion of the small vessels results in lacunar cerebral infarction, and non-occlusive arteriopathy causes chronic cerebral hypoperfusion and WM lesions (Pantoni and Garcia, 1997). Indeed, WM lesions can be induced by a ligation of the bilateral common carotid arteries (CCAs) in rats, which leads to a 50–70% decrease in normal cerebral blood flow (CBF) over an extended period of time (Tsuchiya

Corresponding author. Fax: +81 75 751 3766.
E-mail address: tomimoto@kuhp.kyoto-u.ac.jp (H. Tomimoto).

Abbreviations: WM, white matter; CVD, cerebrovascular disease; CCAs, common carotid arteries; CBF, cerebral blood flow; iNOS, inducible nitric oxide synthase; PBS, phosphate-buffered saline; KB, Klüver–Barrera; BBB, blood–brain barrier; TNF , tumor necrosis factor alpha; COX2, cyclooxygenase 2

0006-8993/$ – see front matter © 2006 Elsevier B.V. All rights reserved.
doi:10.1016/j.brainres.2006.11.084

et al., 1992; Wakita et al., 1994). The myelins become rarefied with a proliferation of the astroglia and an activation of microglia, plus oligodendroglial cell death with DNA fragmentation in the WM (Tomimoto et al., 2003).

S100 is a 20-kDa Ca-binding protein composed of and subunits, and is primarily expressed by astroglia in the brain. This protein may play a dual role in the regulation of cell function, being beneficial to cells at low doses but detrimental at high doses (Hu et al., 1996). In human CVD, a significant correlation has been reported between the plasma concentration of S100 protein and the volume of the cerebral infarct (Aurell et al., 1991). Although low concentrations of S100 protein protect cultured neurons from glutamate-induced excitotoxic damage, a high concentration of this protein upregulates the expression of inducible nitric oxide synthase (iNOS) in cultured astroglia with the subsequent production of NO and death of astroglia and neurons (Hu et al., 1996, 1997; Murphy, 2000).

Indeed, arundic acid, an agent that inhibits the astrocytic synthesis of S100 (Asano et al., 2005), has been shown to be neuroprotective in a rat model of acute cerebral infarction (Tateishi et al., 2002). Arundic acid may interfere with the intricate pathways of astrocytic activation upstream to the mRNA expression of various proteins, and is considered to be a modulator of the gene expression and functions of astroglia (Asano et al., 2005; Shinagawa et al., 1999).

In the present study, we examined the protective effects of arundic acid on WM lesions during chronic cerebral hypoperfusion, and also investigated its therapeutic window for delayed treatment. Our results support the potential use of arundic acid as a therapeutic intervention in human cerebrovascular WM lesions with cognitive impairment.

2. Results

2.1. *Mortality rates and laboratory data*

In the first series of experiments, 1 out of 7 arundic acid-treated rats died at a dosage of 5.0 mg/kg (14.3%), and none died at dosages of 10.0 and 20.0 mg/kg (0.0%). The laboratory data (erythrocyte count, leukocyte count, GOT, GPT, BUN and creatinine levels) and rectal temperature were not significantly different between the vehicle-treated and arundic acid-treated rats (Table 1).

2.2. *Dose-dependent effect of arundic acid on S100 protein expression*

In the WM of the sham-operated animals, only a few astroglia showed positive immunostaining for the S100 protein. From 3 to 14 days after the operation, the brains of the vehicle-treated animals showed a numerical increase in astroglia, which were immunoreactive for S100 protein in various WM regions such as the optic nerve, optic tract, corpus callosum, and internal capsule (Figs. 1A–D). These S100 protein-immunoreactive astroglia increased in number after BCAO as compared to the sham-operated control group in these WM regions (Fig. 1E, Table 2).

In the 10.0 and 20.0 mg/kg arundic acid-treated rats, S100 protein-immunoreactive astroglia appeared to be less numerous in the WM regions as compared to the vehicle-treated animals for 14 days. In the semi-quantitative analysis, the number of S100 protein-immunoreactive astroglia was reduced in both 10.0 and 20.0 mg/kg arundic acid-treated groups as compared to the vehicle-treated group ($p<0.001$; Figs. 2A–D). The number of astroglia decreased in the 5.0, 10.0 and 20.0 mg/kg arundic acid-treated groups compared to the vehicle-treated group. The number was also reduced in the 20.0 mg/kg arundic acid-treated animals as compared to the 10.0 mg/kg arundic acid-treated animals ($p<0.05$), indicating a dose-dependent effect for arundic acid (Fig. 2E, Table 2).

2.3. *Dose-dependent effect of arundic acid on WM lesions*

This dose-related protective effect was similarly observed with respect to the WM lesions. In the 10.0 and 20.0 mg/kg arundic acid-treated groups, the scores were lower as compared to the vehicle-treated group (two-factor factorial ANOVA; $p<0.001$). There were no significant differences in grading scores between the 5.0 mg/kg arundic acid-treated group and vehicle-treated group. However, the 20.0 mg/kg arundic acid-treated animals showed a significant reduction ($p<0.05$) as compared to the 10.0 mg/kg arundic acid-treated animals (Fig. 2F, Table 2).

2.4. *Effects of delayed treatment*

In the delayed-treatment group, which started from 1, 3, or 7 days after the operation, the number of S100 protein-immunoreactive astroglia showed a significant decrease in the WM regions as compared to the vehicle-treated animals

Table 1 – Summary of the laboratory data in rats receiving vehicle or arundic acid

	Erythrocyte ($\times10^4$/mm^3) ($n=6$)	Leukocyte ($\times10^2$/mm^3) ($n=6$)	Thrombocyte ($\times10^3$/mm^3) ($n=6$)	GOT (IU/l) ($n=5$)	GPT (IU/l) ($n=6$)	BUN (mg/dl) ($n=5$)	Creatinine (mg/dl) ($n=6$)	Rectal temperature (°C) ($n=6$)
Vehicle	753.0±42.8	48.4±8.6	88.6±9.6	156.8±18.8	53.6±6.6	20.4±2.8	0.48±0.08	36.5±0.5
Arundic acid (5.0 mg/kg)	790.0±36.8	52.5±22.8	90.4±10.8	178.6±20.4	49.6±8.8	21.8±2.2	0.54±0.12	36.6±1.0
Arundic acid (10.0 mg/kg)	778.0±20.4	50.8±16.8	92.4±9.6	148.8±22.4	45.2±6.8	18.6±1.9	0.46±0.09	36.5±1.0
Arundic acid (20.0 mg/kg)	774.4±31.8	54.8±18.6	91.4±14.4	166.6±38.4	51.2±9.2	19.8±2.4	0.52±0.14	36.6±0.5

Values represent means±SD. n, number of animals. No significant differences were detected in the laboratory data between the arundic acid-treated group and the vehicle-treated group.

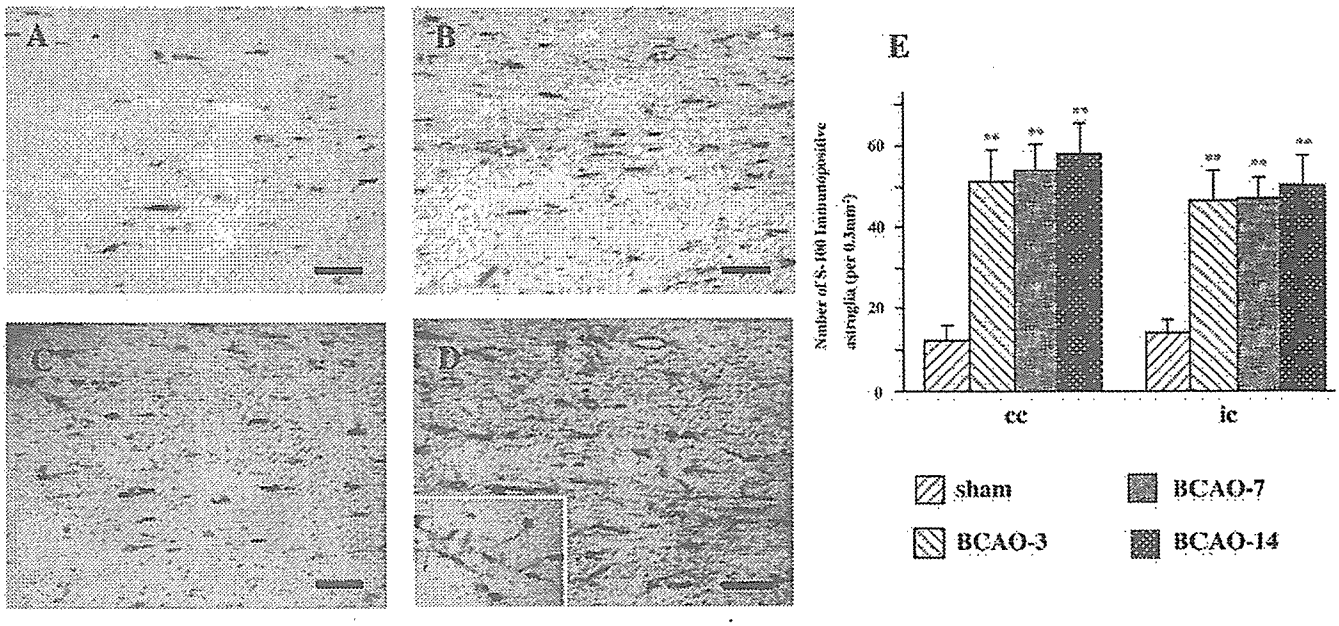

Fig. 1 – Photomicrographs of the immunohistochemical staining for S100 protein in the corpus callosum. The rats were subjected to a sham operation (A), or bilateral ligation of the carotid arteries for 3 days (B), 7 days (C) or 14 days (D). An inset in (D) indicates that S100 protein is intensely expressed in astroglial foot processes around the blood vessel. Bars indicate 100 m. E: Histograms of the numerical densities of S100 protein-immunoreactive astroglia in the WM of the rats after a bilateral common carotid artery occlusion. Six animals were used in each group. The asterisks indicate statistical significance at $p<0.01$ by Mann–Whitney *U* test when compared with the sham-operated controls. cc, corpus callosum; ic, internal capsule.

for 14 days (Figs. 3A–E, Table 2). The WM lesions were less severe (two-factor factorial ANOVA; $p<0.001$) as compared to the vehicle-treated group in the groups starting at 1 day and 3 days after the operation (Fig. 3F, Table 2), but there were no significant changes in the group starting at 7 days.

3. Discussion

In the present study, we demonstrated a protective effect for arundic acid against astroglial activation and WM lesions during chronic cerebral hypoperfusion. Arundic acid suppressed both the activation of the astroglia and the WM lesions in a dose-dependent manner. Both the astroglial activation and WM lesions were suppressed at dosages over 10 mg/kg, whereas the dosage of 5.0 mg/kg suppressed the astroglial activation exclusively. Therefore, it is unlikely that the activation of the astroglia was secondary to the WM damage, but rather seems to be related to the causative mechanism.

Microglia and astroglia are activated in the WM aberrantly after chronic cerebral hypoperfusion (Wakita et al., 1994). This activation occurs in a manner that predicts the extent and severity of the subsequent WM damage, suggesting an important role of glial activation in the pathogenesis of WM lesions. In the susceptible WM, apoptosis of the oligodendroglia is induced with an upregulation of inflammatory cytokines including tumor necrosis factor alpha (TNF), and free radicals released from activated microglia and astroglia (Tomimoto et al., 2003). In addition, the compromised BBB (Ueno et al., 2002) may allow the entry of macromolecules and other blood constituents such as proteases, immunoglobulins, complements, and cytokines into the perivascular WM tissues.

In studies using a neuronal and astroglia co-culture system, a high concentration of S100 protein upregulated NO release from the astroglia, which was shown to be neurotoxic

Table 2 – The number of S100 protein-immunoreactive astroglia in the white matter

	Corpus callosum				Internal capsule			
I. Temporal profile after BCAO	Sham	3 days	7 days	14 days	Sham	3 days	7 days	14 days
	12.3±3.5	51.3±7.8	53.8±6.9	58.1±7.3	14.0±3.6	46.5±7.7	47.0±5.2	50.5±7.1
II. Dose-dependent effect	Vehicle	5 mg/kg	10 mg/kg	20 mg/kg	Vehicle	5 mg/kg	10 mg/kg	20 mg/kg
	63.5±8.3	53.1±6.3	35.3±6.2	10.9±6.0	54.9±8.4	33.0±7.1	26.1±5	21.9±5.7
III. Effects of delayed treatment	Vehicle	Day 1	Day 3	Day 7	Vehicle	Day 1	Day 3	Day 7
	62.0±6.6	13.2±3.8	18.2±5.1	48.9±6.6	54.5±7.1	21.9±3.1	23.7±5.0	42.2±6.3

Values represent the number of S100 protein-immunoreactive astroglia in 0.3 mm^2 (means±SD).
$p<0.01$ compared to the sham-operated (I) and the vehicle-treated (II and III) animals.

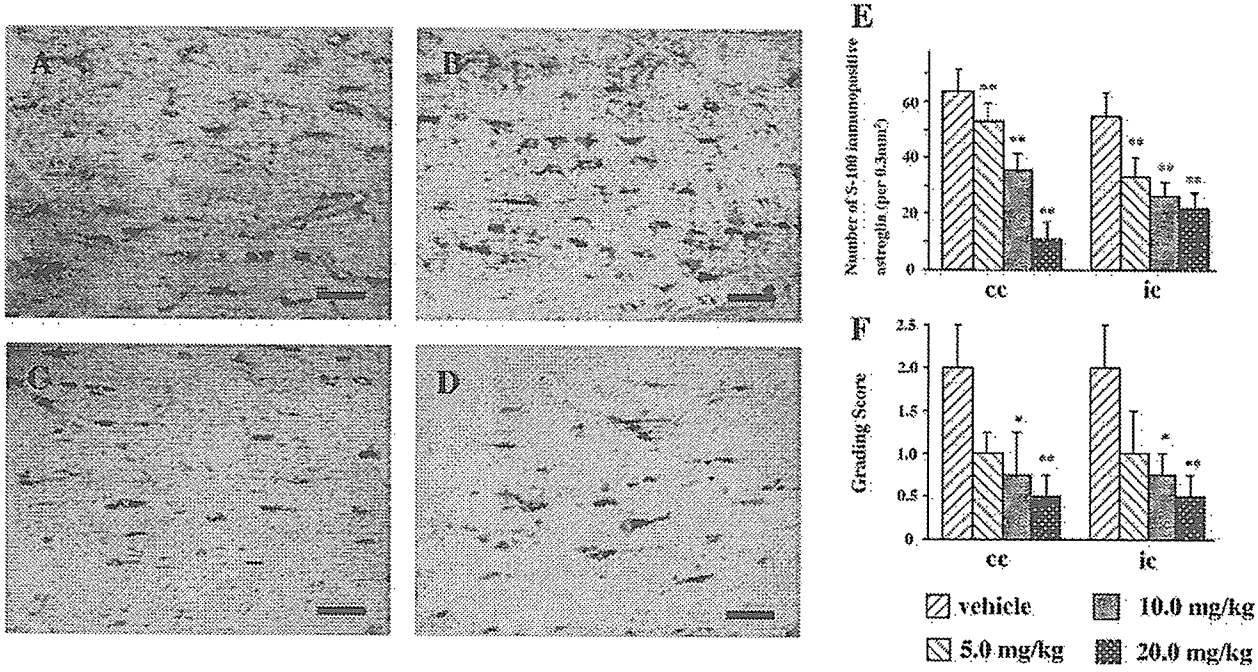

Fig. 2 – Photomicrographs of the immunohistochemical staining for S100 protein in the corpus callosum. The animals received an intraperitoneal injection of vehicle (A) or 5.0 mg/kg (B), 10.0 mg/kg (C) and 20.0 mg/kg (D) of arundic acid for 14 days. In the arundic acid-treated animals, astroglia immunoreactive for S100 protein were less numerous as compared with the vehicle-treated animals. Bars indicate 100 m. The histograms show the numerical densities of S100 protein-immunoreactive astroglia (E), and the grading scores for the WM lesions (F) in rats receiving either vehicle or arundic acid for 14 days. $^{*}p<0.05$; $^{**}p<0.01$ by Fisher's protected least significant difference procedure, as compared to the vehicle-treated animals.

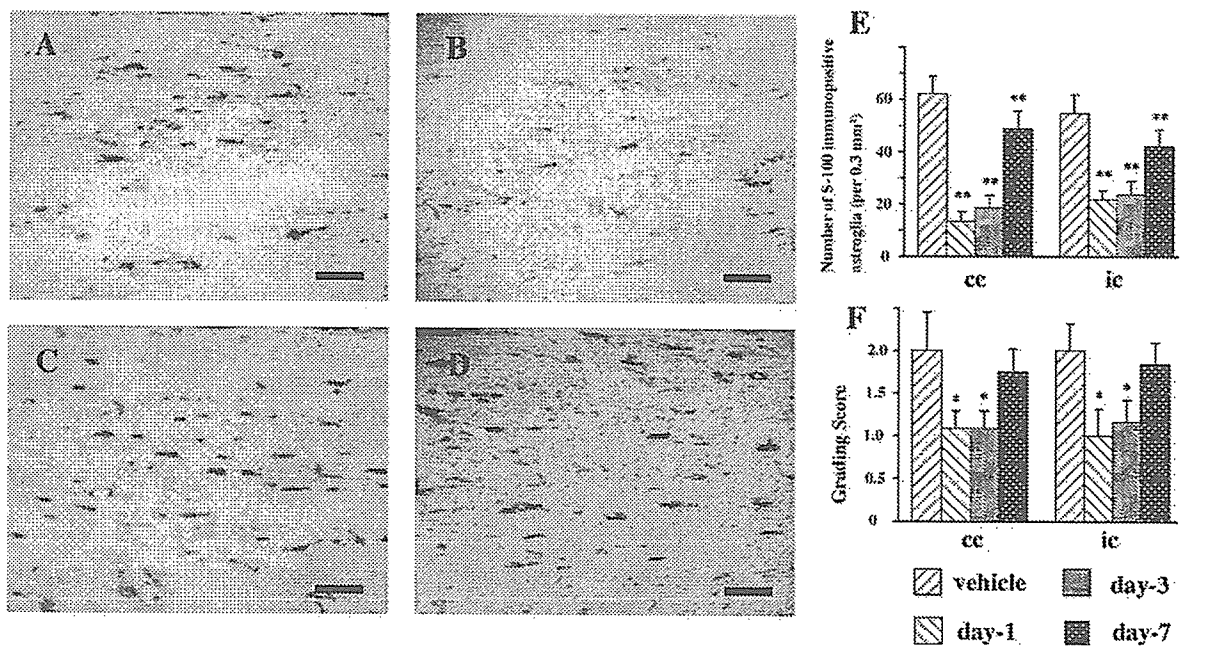

Fig. 3 – Photomicrographs of the immunohistochemical staining for S100 protein in the corpus callosum. The animals received an intraperitoneal injection of 20.0 mg/kg of arundic acid from 1 day (B), 3 days (C) or 7 days (D) after the operation, until 14 days. The control animals (A) received a daily injection of vehicle 1 day before the operation until 14 days. In the delayed treatment with arundic acid, the number of S100 protein-immunoreactive astroglia was significantly reduced as compared with the control animals. Bars indicate 100 m. The histograms show the numerical density of S100 protein-immunoreactive astroglia (E) and the grading scores for the WM lesions (F) in rats receiving either vehicle or arundic acid from 1 day, 3 days or 7 days after the operation until 14 days. $^{*}p<0.05$; $^{**}p<0.01$ by Fisher's protected least significant difference procedure, as compared to the vehicle-treated animals.

(Hu et al., 1997; Nawashiro et al., 2000). Although the mechanism of responsible for this astroglial activation by a low concentration of S100 protein remains unclear, this protein is believed to be further activated by a positive feedback loop (Guo et al., 2001; Murphy, 2000). It is postulated that these excessively activated astroglia may cause secondary tissue damage by the production of cytotoxic cytokines such as TNF , and cyclooxygenase 2 (COX2) and iNOS (Lam et al., 2001; Sharp et al., 2000). Indeed, the delayed expansion of the cerebral infarction was accompanied by astroglial activation as well as by an increased tissue level of S100 protein in the peri-infarct area. Thus, the astroglial overexpression of S100 protein is considered to play a pivotal role in infarct expansion by causing alterations in the activities of multiple intracellular signaling pathways and the expression of various downstream proteins (Asano et al., 2005; Matsui et al., 2002).

Several *in vitro* and *in vivo* studies have determined the pharmacological actions of arundic acid on astroglia. Arundic acid acts selectively on astroglia and modulates their activation, or prevents excessive activation that may be harmful to neighboring neurons. It does not act on neuronal cultures directly, but suppresses the changes induced in the co-cultured astroglia, such as an increase in S100 content, the secretion of nerve growth factor, a reduction in glutamate transporter (GLT-1 and GLAST) expression and the disappearance of GABAA receptors, in a dose-dependent manner, without affecting GFAP expression (Asano et al., 2005; Himeda et al., 2006; Katsumata et al., 1999; Matsui et al., 2002). In addition, arundic acid inhibits the expression of cyclooxygenase-2 or inducible nitric oxide synthase mRNA induced by lipopolysaccharide in cultured astroglia (Shimoda et al., 1998).

The dosage ranging from 5 to 20 mg/kg in the present study was comparable to that used in clinical application (8 mg/kg/h in acute stroke patients) (Pettigrew et al., in press). Furthermore, arundic acid was effective in delayed treatment starting from 7 days in terms of astroglial activation, and 3 days in terms of the WM lesions. This broad therapeutic time window is of clinical relevance, because the patients with subcortical vascular dementia, a form of vascular dementia characterized by diffuse WM lesions, frequently undergo a latent deterioration and hospitalization delay (Roman, 2005).

4. Experimental procedures

4.1. *Animals*

Chronic cerebral hypoperfusion was induced in male Wistar rats (150 to 200 g; Shimizu Laboratory Supplies Co. Ltd., Kyoto, Japan) as previously described (Wakita et al., 1994). The animals were anesthetized with sodium pentobarbital (25 mg/kg, i. p.) and were allowed spontaneous respiration throughout the surgical procedure. Through a midline cervical incision, both CCAs were exposed and double-ligated with silk sutures. Their rectal temperature was monitored and maintained between 36.0 and 37.0 °C during the surgical procedure, and the rats were kept in animal quarters with standard rodent chow and tap water *ad libitum* after the operation.

4.2. *Treatment with arundic acid*

The rats with vehicle (saline) treatment were sacrificed at 3, 7 and 14 days (body weight, 300 g; $n=6$, for each group) to study the temporal profile of the S100 protein-immunoractive astroglia and the WM lesions. In the first series of experiments with arundic acid, the animals received a daily intraperitoneal injection of 5.0, 10.0 or 20.0 mg/kg of arundic acid, or vehicle, from 1 day before the operation to 14 days afterwards ($n=6$ for each group). At 14 days after ligation, the animals were sacrificed and subjected to the experiments detailed below. The sham-operated animals were treated similarly to the operated ones, except the CCAs were not occluded. In the second series with a delayed-treatment, the animals received a daily intraperitoneal injection of 20.0 mg/kg of arundic acid or vehicle from 1 day, 3 days or 7 days after the operation until 14 days ($n=6$ for each group). At 14 days after ligation, the animals were sacrificed and subjected to the experiments detailed below. The control animals received a daily injection of vehicle 1 day after the operation until 14 days.

4.3. *Standard histological and immunohistochemical study*

After the operation, the animals were deeply anesthetized with sodium pentobarbital and were perfused transcardially with 0.01 mol/L phosphate-buffered saline (PBS), and then with a fixative containing 4% paraformaldehyde and 0.2% picric acid in 0.1 mol/L PB (pH 7.4). The brains were then stored in 20% sucrose in 0.1 mol/L PBS (pH 7.4). These specimens were embedded in paraffin and sliced into 2 m-thick coronal sections. Klüver–Barrera (KB) staining was used to observe any histological changes. The severity of the WM lesions was graded as normal (grade 0), disarrangement of the nerve fibers (grade 1), formation of vacuoles (grade 2) and loss of myelinated fibers (grade 3) by two independent investigators blinded to the type of treatment, as described elsewhere (Wakita et al., 1994). For the immunohistochemistry, polyclonal antibodies directed against the S100 protein (diluted 1:1000; Dakopatts, 4.5 mg/L) were used in the present study. After incubation with the primary antibodies, the sections were treated with a biotinylated anti-rabbit antibody (IgG) (diluted 1:200; Vector Laboratories), and an avidin biotin complex (diluted 1:200; Vector Laboratories) in 20 mmol/L PBS containing 0.3% Triton-X. The sections were finally incubated in 0.01% diaminobenzidine tetrahydrochloride and 0.005% H_2O_2 in 50 mmol/L Tris HCl (pH 7.6). To test the specificity of the immunohistochemical reaction, coronal sections were treated with normal mouse IgG instead of the primary antibodies. The number of nuclei with S100 protein-immunoreactive cytoplasm was counted against a square test grid in 20 representative fields (per 0.3 mm^2) of the corpus callosum and internal capsule ($n=6$) by two independent investigators blinded to the type of treatments as described previously (Tomimoto et al., 1996).

4.4. *Statistical analysis*

The data were expressed as means±SD. Differences in rectal temperature between the groups were determined by a

repeated-measure ANOVA. Differences in terms of laboratory blood data were determined by a one-factor ANOVA between each group. Differences in the grading scores were determined by a two-factor factorial ANOVA followed by Fischer's protected least significant difference procedure between each group. The Kruskal–Wallis test followed by post-hoc test was used to compare the ischemic group with the sham-operated control group in the semiquantification for S100 protein-immunoreactive astroglia. A p value of <0.05 was considered to be statistically significant.

Acknowledgments

We appreciatively acknowledge Ono Pharmaceutical Co. Ltd., Osaka, Japan, for providing arundic acid (ONO-2506), and for helpful advice. This study was supported by a grant-in-aid for scientific research (C) (18590936) from the Japanese Ministry of Education, Culture, Sports, Science and Technology to H. T. and Dr. H. Saiki (Kitano Hospital, Osaka, Japan).

REFERENCES

Asano, T., Mori, T., Shimoda, T., Shinagawa, R., Satoh, S., Yada, N., Katsumata, S., Matsuda, S., Kagamiishi, Y., Tateishi, N., 2005. Arundic acid (ONO-2506) ameliorates delayed ischemic brain damage by preventing astrocytic overproduction of S100B. Curr. Drug Targets, CNS Neurol. Disord. 4, 127–142.

Aurell, A., Rosengren, E.L., Larlsson, B., Olsson, E.J., Zbornikova, V., Haglid, G.K., 1991. Determination of S-100 and glial fibrillary acidic protein concentrations in cerebrospinal fluid after brain infarction. Stroke 22, 1254–1258.

Guo, L., Sawkar, A., Zasadzki, M., Watterson, M.D., 2001. Similar activation of glial cultures from different rat brain regions by neuroinflammatory stimuli and downregulation of the activation by a new class of small molecule ligands. Neurobiol. Aging 22, 975–981.

Himeda, T., Kadoguchi, N., Kamiyama, Y., Kato, H., Maegawa, H., Araki, T., 2006. Neuroprotective effect of arundic acid, an astrocyte-modulating agent, in mouse brain against MPTP (1-methyl-4-phenyl-1,2,3,6-tetrahydropyridine) neurotoxicity. Neuropharmacology 50, 329–344.

Hu, J., Castets, F., Guevana, L.J., 1996. S100 stimulates inducible nitric oxide synthase activity and mRNA levels in rat cortical astrocytes. J. Biol. Chem. 271, 2543–2547.

Hu, J., Ferreia, A., 1997. S100 induces neuronal cell death through nitric oxide release from astrocytes. J. Neurochem. 69, 2294–2301.

Katsumata, S., Tateishi, N., Kagamiishi, Y., Shintaku, K., Hayakawa, T., Shimoda, T., Shinagawa, R., Akiyama, T., Katsube, N., 1999. Inhibitory effect of ONO-2506 on GABAA receptor disappearance in cultures astrocytes and ischemic brain. Abstr.-Soc. Neurosci. 25, 2108.

Lam, G.A., Koppal, T., Akama, T.K., Guo, L., Craft, M.J., Samy, B., Schavocky, P.J., Watterson, M.D., 2001. Mechanism of glial activation by S100B: involvement of the transcription factor NF B. Neurobiol. Aging 22, 765–772.

Matsui, T., Mori, T., Tateishi, N., Kagamiishi, Y., Satoh, S., Katsube, N., Morizawa, E., Morimoto, T., Ikuda, F., Asano, T., 2002. Astrocytic activation and delayed infarct expansion after permanent focal ischemia in rats. Part 1: enhanced astrocytic synthesis of S100 in the periinfarct area precedes delayed infarct expansion. J. Cereb. Blood Flow Metab. 22, 711–722.

Murphy, S., 2000. Production of nitric oxide by glial cells: regulation and potential roles in the CNS. Glia 29, 1–13.

Nawashiro, H., Brenner, M., Fukui, S., Shima, K., Hallenbeck, M.J., 2000. High susceptibility to cerebral ischemia in GFAP-null mice. J. Cereb. Blood Flow Metab. 20, 1040–1044.

Pantoni, H.J., Garcia, H.J., 1997. Pathogenesis of leukoaraiosis: a review. Stroke 28, 652–659.

Pettigrew, C.L., Kasner, E.S., Albers, W.G., Gorman, M., Grotta, C.J., Sherman, G.D., Funakoshi, Y., Ishibashi, H., for the arundic acid (ONO-2506) stroke study group, 2006. Safety and tolerability of arundic acid in acute ischemic stroke. J. Neurol. Sci. 251, 50–56.

Roman, C.G., 2005. Vascular dementia prevention: a risk factor analysis. Cerebrovasc. Dis. 20, 91–100.

Sharp, R.F., Lu, A., Tang, Y., Millhorn, E.D., 2000. Multiple molecular penumbras after focal cerebral ischemia. J. Cereb. Blood Flow Metab. 20, 1011–1032.

Shimoda, T., Tateishi, K., Shintaku, K., Yada, N., Katagi, J., Akiyama, T., Maekawa, H., Shinagawa, R., Kondo, K., 1998. ONO-2506, a novel astrocyte modulating agent, suppresses of COX-2 and iNOS mRNA expression in cultured astrocytes and ischemic brain. Abstr.-Soc. Neurosci. 24, 384.

Shinagawa, R., Tateishi, N., Shimoda, T., Maekawa, H., Yada, N., Akiyama, T., Matsuda, S., Katsube, N., 1999. Modulating effects of ONO-2506 on astrocytic activation in cultured astrocytes from rat cerebrum. Abstr.-Soc. Neurosci. 25, 843.

Tateishi, N., Mori, T., Kagamiishi, Y., Satoh, S., Katsube, N., Morizawa, E., Morimoto, T., Matsui, T., Asano, T., 2002. Astrocytic activation and delayed infarct expansion after permanent focal ischemia in rats. part 2: suppression of astrocytic activation by a novel agent (R)-(–)-2-propyloctanoic acid (ONO-2506) leads to mitigation of delayed infarct expansion and early improvement of neurologic deficits. J. Cereb. Blood Flow Metab. 22, 723–734.

Tomimoto, H., Akiguchi, I., Suenaga, T., Nishimura, M., Wakita, H., Nakamura, S., Kimura, J., 1996. Alterations of the blood–brain barrier and glial cells in white matter lesions in cerebrovascular and Alzheimer's disease patients. Stroke 27, 2069–2074.

Tomimoto, H., Ihara, M., Wakita, H., Ohtani, R., Lin, X.J., Akiguchi, I., Kinoshita, M., Shibasaki, H., 2003. Chronic cerebral hypoperfusion induces white matter lesions and loss of oligodendroglia with DNA fragmentation in the rat. Acta Neuropathol. (Berl.) 106, 527–534.

Tsuchiya, M., Sako, K., Yura, S., Yonemasu, Y., 1992. Cerebral blood flow and histopathological changes following permanent bilateral carotid artery ligation in Wistar rats. Exp. Brain Res. 89, 87–92.

Ueno, M., Tomimoto, H., Akiguchi, I., Wakita, H., Sakamoto, H., 2002. Blood–brain barrier is disrupted in the white matter lesions in a rat model of chronic cerebral hypoperfusion. J. Cereb. Blood Flow Metab. 22, 97–104.

Wakita, H., Tomimoto, H., Akiguchi, I., Kimura, J., 1994. Glial activation and white matter changes in the rat brain induced by chronic cerebral hypoperfusion: an immunohistochemical study. Acta Neuropathol. (Berl.) 87, 484–492.

BRAIN RESEARCH 1136 (2007) 219–227

available at www.sciencedirect.com

ScienceDirect

www.elsevier.com/locate/brainres

BRAIN RESEARCH

Research Report

Accumulation of Hsc70 and Hsp70 in glial cytoplasmic inclusions in patients with multiple system atrophy

Yasuhiro Kawamoto[a,*], *Ichiro Akiguchi*[a], *Yoshitomo Shirakashi*[a], *Yasuyuki Honjo*[a], *Hidekazu Tomimoto*[a], *Ryosuke Takahashi*[a], *Herbert Budka*[b]

[a]*Department of Neurology, Faculty of Medicine, Kyoto University, 54 Shogoin-Kawaharacho, Sakyoku, Kyoto 606-8507, Japan*
[b]*Institute of Neurology, Medical University Vienna, Vienna, Austria*

ARTICLE INFO

Article history:
Accepted 9 December 2006
Available online 22 December 2006

Keywords:
-Synuclein
Glial cytoplasmic inclusion
Hsc70
Hsp70
Multiple system atrophy

ABSTRACT

Heat shock proteins (HSPs) are molecular chaperones which can be induced by several kinds of stresses, and Hsc70 and Hsp70 are two major members of the family of 70 kDa HSPs. A major component of Lewy bodies (LBs) is -synuclein, and Hsp70 has been observed in the LBs of brains with Parkinson's disease. Hsp70 has also been demonstrated to have the ability to suppress -synuclein toxicity *in vitro* and *in vivo*. To investigate the precise role of Hsc70 and Hsp70 in patients with multiple system atrophy (MSA), which is another -synuclein-related disease, we performed immunohistochemical studies on Hsc70 and Hsp70 using autopsied brains from 7 normal subjects and 15 patients with MSA. In the normal human brains, both neurons and glial cells, including oligodendrocytes, showed only weak Hsc70 and Hsp70 immunoreactivities. In contrast, in the brains with MSA, numerous glial cytoplasmic inclusions (GCIs) were intensely immunostained with Hsc70, and strong Hsc70 immunoreactivity was also found in glial intranuclear inclusions (GNIs), neuronal cytoplasmic inclusions (NCIs) and neuronal intranuclear inclusions (NNIs) as well as dystrophic neurites. The immunolabeling pattern for Hsp70 in the MSA brains was slightly different from that of Hsc70, and Hsp70 immunoreactivity was observed in many reactive astrocytes as well as some glial and neuronal inclusions. Our results suggest that the widespread accumulation of Hsc70 and Hsp70 may occur in brains with MSA, and that Hsc70 and Hsp70 may be associated with the pathogenesis of MSA.

1. Introduction

Multiple system atrophy (MSA) is a single nosological entity which encompasses olivopontocerebellar atrophy (OPCA), striatonigral degeneration (SND) and Shy–Drager syndrome (SDS) (Graham and Oppenheimer, 1969). MSA is characterized clinically by varying degrees of autonomic failure, cerebellar ataxia, parkinsonism and pyramidal tract signs (Wenning et al., 1994). Recently, MSA has been divided into two groups: one group contains those patients with predominant cerebellar features

Corresponding author. Fax: +81 75 751 3265.
E-mail address: kawamoto@kuhp.kyoto-u.ac.jp (Y. Kawamoto).

Abbreviations: BCIP/NBT, 5-bromo-4-chloro-3-indolyl-phosphate/nitroblue tetrazolium; GCIs, glial cytoplasmic inclusions; GNIs, glial intranuclear inclusions; HSPs, heat shock proteins; LBs, Lewy bodies; MSA, multiple system atrophy; MSA-C, MSA of the cerebellar type; MSA-P, MSA of the parkinsonian type; NCIs, neuronal cytoplasmic inclusions; NNIs, neuronal intranuclear inclusions; OPCA, olivopontocerebellar atrophy; PD, Parkinson's disease; PVDF, polyvinylidene difluoride; SDS, Shy–Drager syndrome; SND, striatonigral degeneration

0006-8993/$ – see front matter © 2006 Elsevier B.V. All rights reserved.
doi:10.1016/j.brainres.2006.12.049

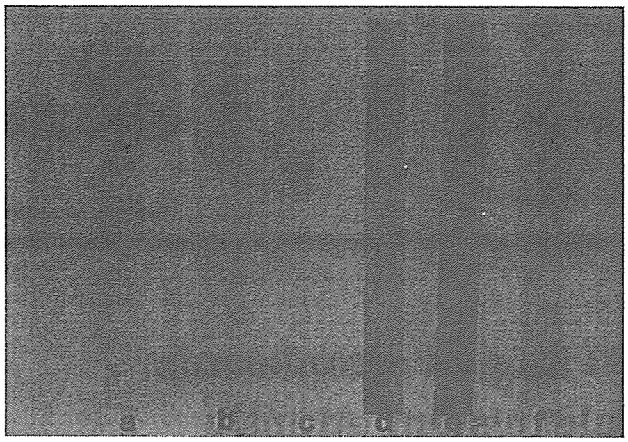

Fig. 1 – Western blot analysis of normal human brain homogenates (a, d), recombinant Hsp70 protein (b, e) and recombinant Hsc70 protein (c, f). Lanes a, b and c were incubated with the anti-Hsc70 antibody, and lanes d, e and f were incubated with the anti-Hsp70 antibody.

(MSA-C), and the other represents patients with predominant parkinsonian features (MSA-P) (Gilman et al., 1999). Specific oligodendroglial cytoplasmic inclusions, which are also referred to as glial cytoplasmic inclusions (GCIs), are the pathological hallmark of MSA (Nakazato et al., 1990; Papp et al., 1989), and the presence of GCIs strongly supports the concept of MSA as a single entity (Papp et al., 1989). GCIs are argyrophilic inclusions that can be detected at high sensitivity by the Gallyas silver staining technique (Papp et al., 1989), and are ultrastructurally composed of loosely packed filaments coated by granular materials (Nakazato et al., 1990; Papp et al., 1989).

Human -synuclein is a presynaptic protein of 140 amino acid residues (Jakes et al., 1994), and missense mutations in the -synuclein gene have been linked to some cases of autosomal dominant familial Parkinson's disease (PD) (Krüger et al., 1998; Polymeropoulos et al., 1997). Lewy bodies (LBs) are neuronal inclusions characteristic for PD (Pollanen et al., 1993), and -synuclein is a major component of both LBs (Spillantini et al., 1997; Wakabayashi et al., 1997, 1998b) and GCIs (Gai et al., 1998; Wakabayashi et al., 1998a,b); therefore, -synuclein-related disorders, including PD and MSA, are now collectively referred to as " -synucleinopathy". In addition to GCIs, -synuclein-immunopositive inclusions are also observed in the neuronal cytoplasm and nuclei of neurons and oligodendrocytes, and they are termed neuronal cytoplasmic inclusions (NCIs), neuronal intranuclear inclusions (NNIs) and glial intranuclear inclusions (GNIs), respectively (Lin et al., 2004; Wakabayashi et al., 1998a,b). Furthermore, a reduction in the solubility of -synuclein has been shown to occur in brains affected by MSA (Dickson et al., 1999; Tu et al., 1998). These data suggest that the neuronal and oligodendroglial accumulation of insoluble -synuclein may be closely related to the pathogenesis of MSA.

Heat shock proteins (HSPs) are molecular chaperones which are induced in response to heat shock, ischemia and other stresses (Ohtsuka and Suzuki, 2000; Sharp et al., 1999). The family of 70 kDa HSPs has two major members: Hsp70, an inducible form, and Hsc70, a constitutively expressed form (Ohtsuka and Suzuki, 2000; Sharp et al., 1999). The localization of Hsp70 in LBs from brains with PD has been previously reported (Auluck et al., 2002; Shin et al., 2005), and Hsp70 has been demonstrated to have the ability to suppress -synuclein toxicity *in vitro* (Dedmon et al., 2005; Klucken et al., 2004) and *in vivo* (Auluck et al., 2002; Klucken et al., 2004). However, the data regarding Hsc70 and Hsp70 in patients with MSA are very limited (Uryu et al., 2006), and therefore, we performed immunohistochemical studies on Hsc70 and Hsp70 using autopsied brains from patients with MSA. We observed the enhanced immunoexpression of both chaperones in those brains affected by MSA.

2. Results

2.1. *Western blot analysis*

A single band at a molecular weight of approximately 70 kDa was immunostained by the anti-Hsc70 antibody in the normal human cerebellar homogenate (Fig. 1a), and the anti-Hsc70 antibody also recognized the recombinant Hsc70 protein (Fig. 1c), but not the recombinant Hsp70 protein (Fig. 1b). On the other hand, a single band of about 70 kDa was immunolabeled with the anti-Hsp70 antibody in the normal human cerebellar homogenate (Fig. 1d), and the anti-Hsp70 antibody reacted with the recombinant Hsp70 antibody (Fig. 1e), but not the recombinant Hsc70 protein (Fig. 1f). Furthermore, both the antibodies detected only a single band of the same molecular weight in the cerebellar homogenate from the patient with MSA (Figs. 2a, b). These results indicate that the anti-Hsc70 and anti-Hsp70 antibodies were specific for human Hsc70 and Hsp70, respectively.

2.2. *Hsc70 and Hsp70 immunoreactivities in normal brains*

In the normal human brains, the neurons generally showed weak Hsc70 immunoreactivity (Fig. 3A), and faint Hsc70

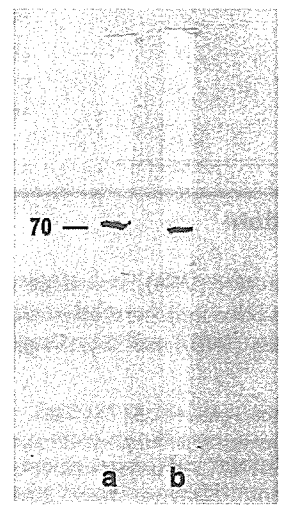

Fig. 2 – Western blot analysis of brain homogenates from the patient with multiple system atrophy. Lanes a and b were incubated with the anti-Hsc70 and anti-Hsp70 antibodies, respectively.

immunoreactivity was observed in a few glial cells, including oligodendrocytes (Fig. 3B).

The immunolabeling pattern of Hsp70 in the normal human brains was similar to that of Hsc70, and both neurons and glial cells were mildly immunoreactive for Hsp70 (Figs. 3C, D).

2.3. *Hsc70 immunoreactivity in brains with MSA*

In contrast to the weak Hsc70 immunoreactivity observed in the oligodendrocytes from the normal brains, numerous GCIs were intensely immunostained with Hsc70 in various lesions of the MSA brains, including the pontine nucleus (Fig. 4A), middle cerebellar peduncle (Fig. 4B) and cerebellar white matter (Fig. 4C). In addition, Hsc70-immunopositive GNIs, which consisted of a few filamentous structures, were found in some oligodendrocytes (Fig. 4D).

Similar to the normal controls, the remaining neurons were generally immunostained weakly in the brains with MSA, but strong Hsc70 immunoreactivity was localized throughout the cell bodies and proximal processes of some neurons (Fig. 4E). In the pontine and inferior olivary nuclei from the MSA cases, NCIs and NNIs in some surviving neurons were intensely immunolabeled (Figs. 4F, G). The NCIs were round or oval in shape (Fig. 4F), and the NNIs were wisps containing several filamentous structures (Fig. 4G). Furthermore, some dystrophic neurites were also densely immunoreactive for Hsc70 (Fig. 4H).

No significant difference was detected in the immunolabeling patterns of the neuronal and oligodendroglial inclusions between the MSA-C and MSA-P cases.

2.4. *Hsp70 immunoreactivity in brains with MSA*

Similar to Hsc70, the GCIs were intensely immunostained with Hsp70 (Figs. 5A, B), but serial sections immunostained alternately with the antibodies against Hsc70 and Hsp70 showed that the proportion of Hsp70-immunopositive GCIs was less than that of Hsc70-positive GCIs. The remaining neurons generally showed weak Hsp70 immunoreactivity (Fig. 5C), and some surviving neurons contained Hsp70-immunopositive NCIs (Fig. 5D). In comparison to Hsc70, the Hsp70-immunolabeled GNIs, NNIs and dystrophic neurites were very few. In addition to the oligodendrocytes, many reactive astrocytes were also strongly immunoreactive for Hsp70 (Fig. 5E), and immunopositive reactive astrocytes were distributed abundantly in the severely affected lesions, where the neuronal loss and astrogliosis were conspicuous (Fig. 5F). Hsp70-immunopositive reactive astrocytes were also observed in the areas where no -synuclein-positive inclusions were found. No significant difference was detected in the immunostaining patterns of the -synuclein-containing inclusions and reactive astrocytes between the MSA-C and MSA-P cases.

2.5. *Double-labeling immunohistochemistry for -synuclein and HSPs*

The double-immunofluorescence staining sections showed that -synuclein and Hsc70 were co-localized in most GCIs (Figs. 6A–C), and the co-localization of -synuclein and Hsp70 was also observed in some GCIs (Figs. 6D–F). No significant differences were detected in the co-localization of -synuclein and Hsc70 or Hsp70 in the GCIs among the cerebellat white matter, pontine base and putamen. The semiquantitative analyses demonstrated that the average percentage of Hsc70- or Hsp70-immunopositive GCIs in the -synuclein-immunolabeled GCIs was approximately 82.1% and 59.8%, respectively.

2.6. *Double-labeling immunohistochemistry for Hsc70 and glial markers*

The double-immunofluorescence staining sections revealed that Hsc70-immunopositive glial cells were mainly transferrin-

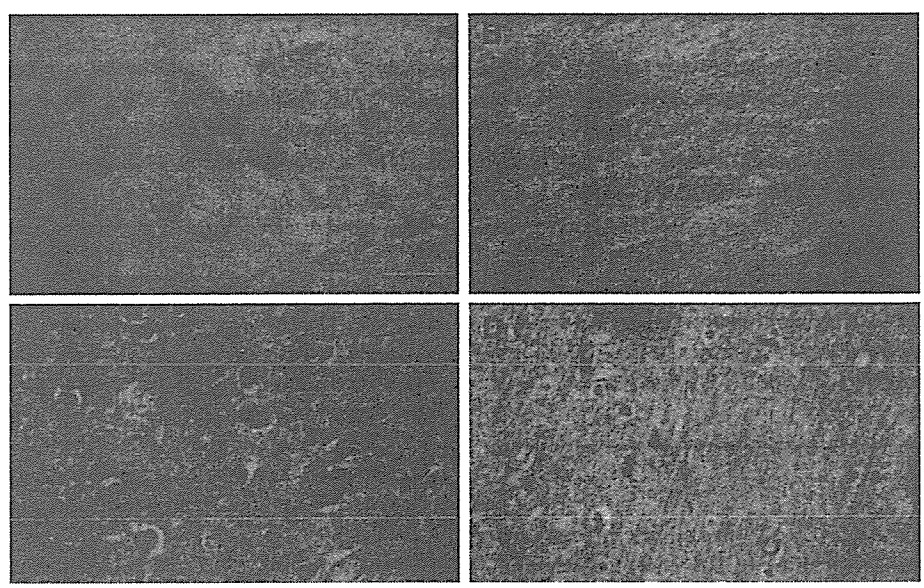

Fig. 3 – Immunohistochemical staining with Hsc70 (A: Control 3; B: Control 5) and with Hsp70 (C: Control 3; D: Control 5) in the normal pontine nucleus (A, C) and cerebellar white matter (B, D). Scale bars=50 m.

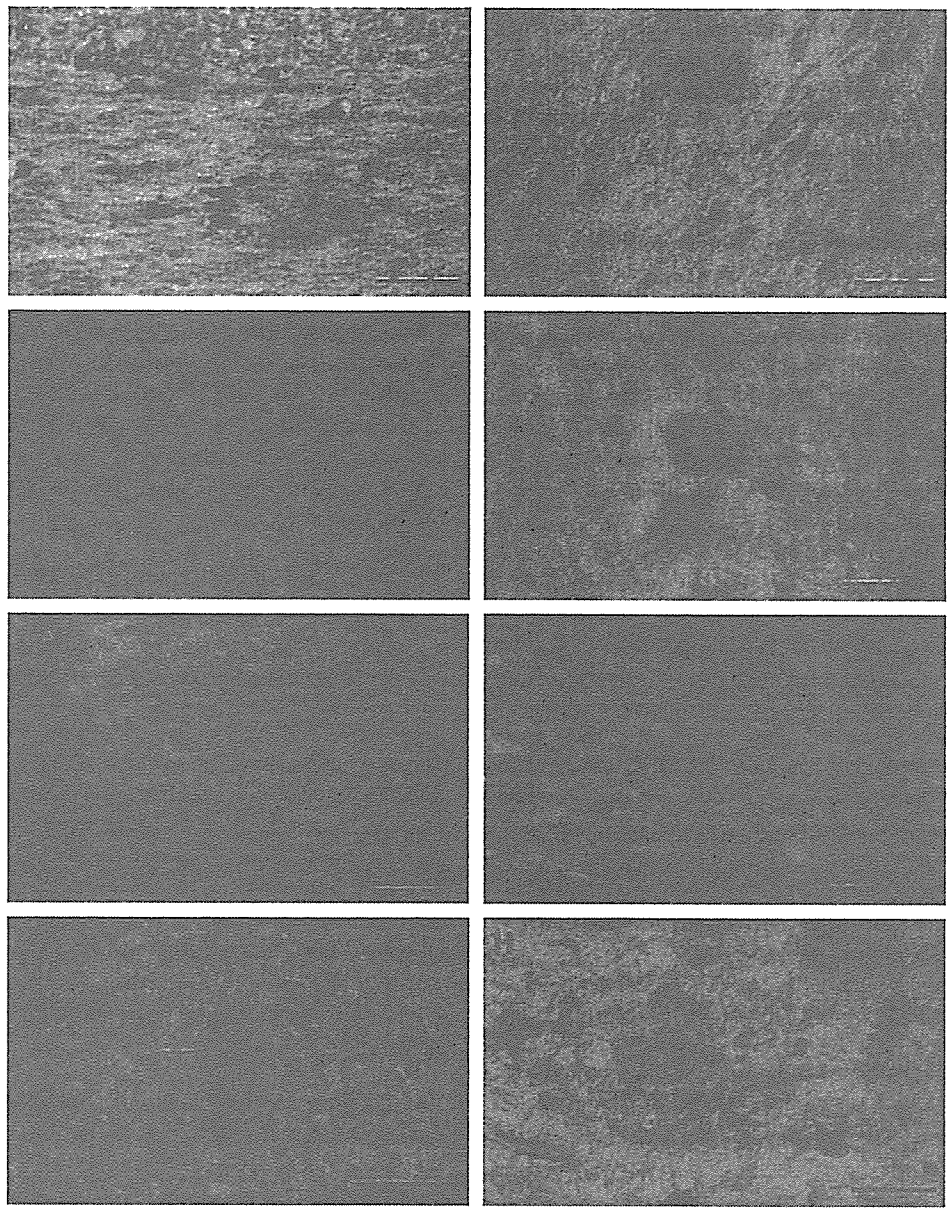

Fig. 4 – Immunohistochemical staining with Hsc70 in the pontine nucleus (A, D-H), middle cerebellar peduncle (B) and cerebellar white matter (C) from the patients with multiple system atrophy (A, C, H: MSA 2; B: MSA 3; D, F, G: MSA 11; E: MSA 14). Note that strong Hsc70 immunoreactivity was observed in the glial cytoplasmic inclusions (GCIs; A–C), glial intranuclear inclusions (GNIs; D, arrow), neuronal cytoplasmic inclusions (NCIs; F), neuronal intranuclear inclusions (NNIs; G, arrow) and dystrophic neurites (H). Scale bars = A–C, E 50 m; D 15 m; F–H 25 m.

positive oligodendrocytes (Figs. 7A–C). In contrast, very few Hsc70-immunopositive structures were located to glial fibrillary acidic protein (GFAP)-positive astrocytes (Figs. 7D–F) and leukocyte common antigen (LCA)-positive microglia (Figs. 7G–I).

3. Discussion

The widespread distribution of GCIs in the central nervous system is the main pathological feature of patients with MSA (Papp and Lantos, 1994). In the present study, we performed immunohistochemical studies on Hsc70 and Hsp70 using autopsied brains from 7 normal subjects and 15 patients with MSA, and then compared the immunostaining patterns between the two groups. We found that a few glial cells, including oligodendrocytes, showed weak Hsc70 and Hsp70 immunoreactivities in the normal brains, but the GCIs were strongly immunoreactive for Hsc70 and Hsp70 in the brains with MSA. Our observations suggest that Hsc70 and Hsp70 may be expressed aberrantly in oligodendrocytes, and may be associated with the formation of GCIs in those brains affected by MSA.

Recently, Uryu et al. (2006) demonstrated that among the various types of HSPs, Hsp90 was most prominently and consistently co-localized with -synuclein in LBs and GCIs, and in contrast to Hsp90, very few GCIs were immunopositive

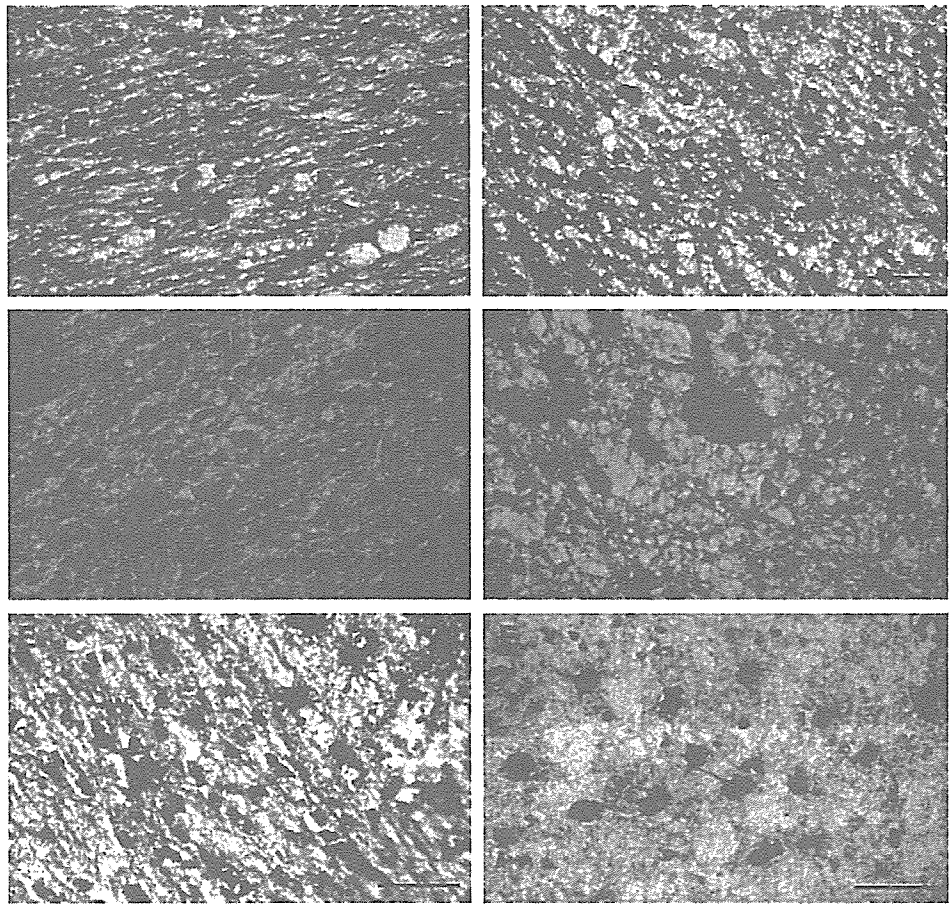

Fig. 5 – Immunohistochemical staining with Hsp70 in the pontine nucleus (A, C, D), cerebellar white matter (B) and putamen (E, F) from the patients with multiple system atrophy (A: MSA 2; B: MSA 3; C, E: MSA 11; D, F: MSA1). Some glial cytoplasmic inclusions (GCIs; A, B) and neuronal cytoplasmic inclusions (NCIs; D) were intensely immunostained. In contrast to the strongly immunopositive GCIs (C, arrows), the remaining neurons showed weak Hsp70 immunoreactivity (C). Reactive astrocytes as well as GCIs were immunoreactive for Hsp70 (E), and immunopositive reactive astrocytes were abundant in the severely affected areas (F). Scale bars = A–C, E, F 50 m; D 25 m.

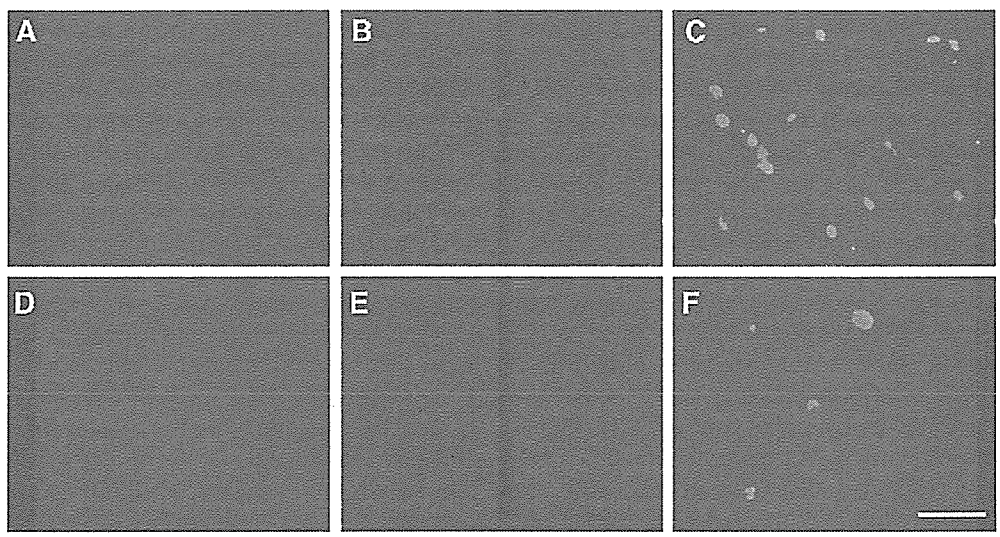

Fig. 6 – Double-immunofluorescence staining for -synuclein (A, D; red) and Hsc70 (B; green) or Hsp70 (E; green) in the cerebellar white matter from the patient with multiple system atrophy (MSA 3). The merged images showed that -synuclein and Hsc70 were co-localized in most glial cytoplasmic inclusions (GCIs; C), and -synuclein and Hsp70 were co-localized in some GCIs (F). Scale bar = F (also for A–E) 20 m.

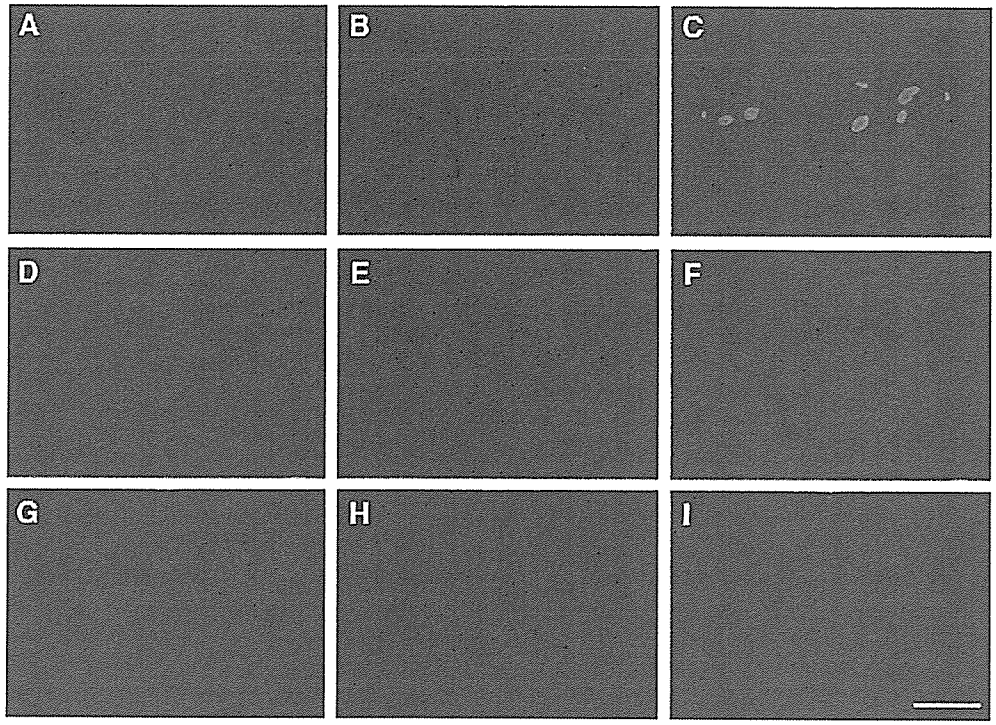

Fig. 7 – Double-immunofluorescence staining for Hsc70 (A, D, G; green) and transferrin (B; red), GFAP (E; red) or LCA (H; red) in the pontine base from the patient with multiple system atrophy (MSA 5). The merged images showed that Hsc70-immunopositive glial cells were mainly oligodendrocytes (C), and very few Hsc70-immunopositive structures were localized to astrocytes (F) and microglia (I). Scale bar=I (also for A–H) 20 m.

for Hsc70 and Hsp70. Conversely, our present results showed that numerous GCIs were strongly immunoreactive for Hsc70, and to a lesser extent for Hsp70. Uryu et al. (2006) reported that they used the anti-Hsc70 and anti-Hsp70 antibodies purchased from W. Welsh. On the other hand, we selected the anti-Hsc70 antibody from Stressgen and the anti-Hsp70 antibody from Santa Cruz Biotechnology, suggesting that the different immunolabeling patterns for Hsc70 and Hsp70 in the GCIs between Uryu's results and our study may be partly due to the properties of the different antibodies.

The accumulation of insoluble -synuclein occurs widely in brains with MSA (Dickson et al., 1999; Tu et al., 1998), and -synuclein immunoreactivity is localized not only to GCIs (Gai et al., 1998; Wakabayashi et al., 1998a,b), but also to GNIs, NCIs, NNIs and dystrophic neurites (Lin et al., 2004; Wakabayashi et al., 1998a,b). In the present study, we observed the same immunolabeling patterns for neuronal and oligodendroglial inclusions between -synuclein and Hsc70, and confirmed the localization of Hsc70 immunoreactivity in GCIs, GNIs, NCIs, NNIs and dystrophic neurites. According to the previous paper (Uryu et al., 2006), co-immunoprecipitation analyses in cultured cells showed that -synuclein interacted predominantly with Hsp90 and Hsc70. Furthermore, Western blot analyses using brain homogenates from patients with -synucleinopathies and -synuclein transgenic mice revealed that Hsp90 and Hsc70 accumulated selectively in the detergent insoluble fractions. These data suggest that both Hsp90 and Hsc70 may be closely related to the formation of these neuronal and oligodendroglial inclusions through their interactions with insoluble -synuclein in brains with MSA.

LBs have been reported to be immunostained with Hsp70 (Auluck et al., 2002; Shin et al., 2005), and recent immunohistochemical studies using anti-Hsc70 and anti-Hsp70 antibodies showed that Hsc70 immunoreactivity in the LBs in nigral neuromelanin-containing neurons from patients with PD was detected more frequently than Hsp70 (Andringa et al., 2006). Our immunohistochemical studies demonstrated that similar to the LBs, Hsc70-immunopositive inclusions were observed more frequently than Hsp70 in those brains with MSA. On the other hand, our studies showed that many reactive astrocytes were intensely immunolabeled with Hsp70 in the brains with MSA, but only a few reactive astrocytes were immunopositive for Hsc70 in the same areas. These results suggest that the ligand of Hsp70 may be different from that of Hsc70, and that there may be a difference between the significance of Hsp70 and Hsc70, and Hsc70 may make a greater contribution to the formation of MSA-related neuronal and oligodendroglial inclusions than Hsp70. Moreover, Hsp70 may be induced more abundantly in reactive astrocytes than Hsc70 in the affected brain areas of patients with MSA.

The aggregation of abnormally misfolded proteins, leading to selective neuronal death, is generally thought to be a common pathological feature of neurodegenerative diseases (Agorogiannis et al., 2004). There are two major protective mechanisms against abnormally misfolded proteins: one is the molecular chaperones which regenerate the misfolded proteins, and the other is the ubiquitin–proteasome system which targets misfolded proteins for degradation and prevents their accumulation (Agorogiannis et al., 2004). GCIs are usually ubiquitinated (Kato et al., 1991; Murayama et al., 1992),

and several chaperone proteins, including B-crystallin (Kato et al., 1991; Murayama et al., 1992), 14-3-3 proteins (Kawamoto et al., 2002; Komori et al., 2003) and Hsp90 (Uryu et al., 2006), have been reported to be localized immunohistochemically to GCIs. Our present results support the immunohistochemical localization of Hsc70 and Hsp70 in GCIs. These results suggest that these two major protective systems may be operating in brains with MSA, and these molecular chaperones, including Hsc70 and Hsp70, may be overexpressed in brains with MSA to regenerate the abnormally misfolded proteins in GCIs, but that these systems may not work well in terms of protein quality control. Furthermore, the accumulation of molecular chaperones in GCIs might cause a lack of these chaperones in surviving neurons in brains with MSA, which may partially contribute to the neuronal cell death. Taken together, further research on the regulation of molecular chaperones, including Hsc70 and Hsp70, will lead to the establishment of new treatments for MSA.

4. Experimental procedures

4.1. *Tissue preparation*

We studied autopsied brains from 7 control subjects without any neurological abnormalities (age range 54–75 years, mean± SD 67.0±7.1 years) and 15 patients with MSA (age range 52–78 years, mean±SD 68.5±7.6 years). These materials were selected from the brain bank at the Neuropathology Laboratories of Kyoto University and Medical University Vienna. Among the 15 patients with MSA, 10 patients were classified as MSA-C and the other 5 patients were MSA-P, and the clinical profiles from all cases are summarized in Table 1. All brains were fixed in 10% neutral formalin for 2 weeks at room temperature. Several paraffin-embedded tissue blocks, including the basal ganglia, brainstem and cerebellum, were prepared and cut into 6- m-thick sections on a microtome. The paraffin-embedded sections were deparaffinized in xylene, followed by rehydration in a decreasing concentration of ethanol solutions. For routine pathological evaluation, the deparaffinized sections from all cases were stained with hematoxylin and eosin, Klüver–Barrera and modified Bielschowsky stains. No histological abnormalities were detected in the sections from all of the control cases, and numerous GCIs were observed in the sections from all MSA cases. The experiments were undertaken with the understanding and written consent of each subject.

Table 1 – Clinical backgrounds of all cases

Case	Age (years)/ Sex	Diagnosis	Duration of illness/ Postmortem delay
Control 1	62/M	Pancreatic carcinoma	NA/3.0 h
Control 2	68/M	Rheumatoid arthritis	NA/2.0 h
Control 3	73/M	Hepatocellular carcinoma	NA/4.5 h
Control 4	68/F	Breast cancer	NA/2.5 h
Control 5	75/M	Pulmonary emphysema	NA/2.0 h
Control 6	69/M	Lung cancer	NA/UD
Control 7	54/M	Pneumonia	NA/2.0 h
MSA 1	78/M	MSA-C	7 years/4.8 h
MSA 2	66/M	MSA-C	4 years/3.5 h
MSA 3	72/F	MSA-C	5 years/2.0 h
MSA 4	71/F	MSA-C	4 years/8.2 h
MSA 5	78/M	MSA-C	3 years/1.8 h
MSA 6	66/M	MSA-C	7 years/1.4 h
MSA 7	76/M	MSA-C	8 years/UD
MSA 8	67/F	MSA-C	2 years/UD
MSA 9	58/F	MSA-C	UD/UD
MSA 10	66/F	MSA-C	UD/UD
MSA 11	52/F	MSA-P	3 years/2.5 h
MSA 12	77/F	MSA-P	5 years/1.4 h
MSA 13	69/F	MSA-P	8 years/6.1 h
MSA 14	72/F	MSA-P	12 years/1.2 h
MSA 15	60/M	MSA-P	6 years/3.5 h

F: female; M: male; MSA: multiple system atrophy; MSA-C: MSA of the cerebellar type; MSA-P: MSA of the parkinsonian type; NA: not applicable; UD: undetermined.

4.2. *Immunohistochemistry*

To examine the immunohistochemical localization of Hsc70 and Hsp70 in normal and MSA human brains, we used a rat anti-Hsc70 monoclonal antibody (SPA-815; Stressgen, Victoria, BC, Canada, 5 g/ml) and a goat anti-Hsp70 polyclonal antibody (K-20; Santa Cruz Biotechnology, Santa Cruz, CA, USA, 2 g/ml). The deparaffinized sections were pretreated with 0.3% hydrogen peroxide (Santoku, Tokyo, Japan) in 0.1 M phosphate-buffered saline (PBS) for 30 min at room temperature to inhibit the endogenous peroxidase activity. After washing with 0.1 M PBS, the sections were blocked with 0.1 M PBS with 3% skimmed milk for 2 h at room temperature. After rinsing with 0.1 M PBS, the anti-Hsc70 or anti-Hsp70 antibody diluted in 0.1 M PBS was applied onto the sections, and the sections were incubated at room temperature overnight in a humidified chamber. After washing with 0.1 M PBS, the sections were reacted with a biotinylated anti-rat or anti-goat IgG (Vector Laboratories, Burlingame, CA, USA) diluted in 0.1 M PBS (1:200) for 1 h at room temperature, followed by an incubation with an avidin–biotin–peroxidase complex kit (Vector Laboratories) diluted in 0.1 M PBS (1:400) for 1 h at room temperature. After rinsing with 0.1 M PBS and then 0.05 M Tris–HCl (pH 7.6), the sections were developed in a colorizing solution containing 0.02% diaminobenzidine tetrahydrochloride (Dojin, Kumamoto, Japan), 0.6% ammonium nickel (II) sulfate (Wako, Osaka, Japan) and 0.005% hydrogen peroxide in 0.05 M Tris–HCl (pH 7.6) for 10 min at room temperature. As negative immunohistochemical controls, some sections were incubated with normal rat or goat serum, and no specific immunopositive staining was detected in these control sections (data not shown).

4.3. *Double immunofluorescence staining*

To compare the anatomical distribution of immunopositive GCIs containing -synuclein and Hsc70 or Hsp70, we performed double-labeling immunohistochemistry using a monoclonal mouse anti- -synuclein antibody (211; Santa Cruz Biotechnology) plus the anti-Hsc70 or anti-Hsp70

antibody. Some sections from the patients with MSA were incubated with the antibodies against -synuclein (211; 4 g/ml) and Hsc70 (SPA-815; 5 g/ml) or Hsp70 (K-20; 2 g/ml) in 0.1 M PBS at room temperature overnight. After washing with 0.01 M PBS, the sections were reacted with secondary antibodies consisting of a tetramethylrhodamine-conjugated rabbit anti-mouse IgG (DakoCytomation, Glostrup, Denmark) and a fluorescein isothiocyanate-conjugated rabbit anti-rat IgG (DakoCytomation) or swine anti-goat IgG (Biosource, Camarillo, CA, USA). After rinsing with 0.01 M PBS, the slides were coverslipped with Vectashield (Vector Laboratories), and viewed with the aid of a fluorescence microscope.

To estimate the proportion of GCIs which were immunoreactive for Hsc70 or Hsp70, we prepared double-immunofluorescence staining sections of the cerebella, pontes and basal ganglia from all patients with MSA. We randomly chose one hundred -synuclein-immunopositive GCIs in the cerebellar white matter, pontine base or putamen of each section from all MSA cases. We then counted the number of Hsc70- or Hsp70-immunopositive GCIs in the one hundred -synuclein-positive GCIs in each section from all MSA cases, and calculated the averaged percentage of Hsc70- and Hsp70-immunopositive GCIs, respectively.

To characterize Hsc70-immunopositive glial cells, we performed double-labeling immunohistochemistry using a mouse monoclonal anti-transferrin antibody (Hytest, Turku, Finland) as a marker for oligodendrocytes, a mouse monoclonal anti-GFAP antibody (DAKO, Glostrup, Denmark) as a marker for astrocytes, and a mouse monoclonal anti-LCA antibody (DAKO) as a marker for microglia. Some sections from the patients with MSA were incubated with the antibodies against Hsc70 (SPA-815; 5 g/ml) and transferrin (1:1000), GFAP (1:1000) or LCA (1:100) in 0.1 M PBS at room temperature overnight. After washing with 0.01 M PBS, the sections were double-immunostained using the same method described above.

4.4. *Characterization of the primary antibodies*

The specificity of the anti-Hsc70 and anti-Hsp70 antibodies was verified by Western blotting using human brain homogenates. Fresh brain tissues were obtained from the cerebellum of an autopsied normal subject (68-year-old male) and an autopsied patient with MSA (66-year-old female). These materials were homogenized in 3 volumes of ice-cold 10 mM PBS containing 1% Nonidet P-40 (Nacalai Tesque, Kyoto, Japan), 0.5% sodium deoxycholate (Difco, Detroit, MI, USA), 0.1% sodium dodecyl sulfate (SDS; Nacalai Tesque), 0.01% phenylmethylsulfonyl fluoride (Nacalai Tesque), 3% aprotinin (Sigma, St Louis, MO, USA) and 1 mM sodium orthovanadate (Sigma). The homogenates were then centrifuged at 15,000 rpm for 15 min at 4 °C, and the supernatants were then mixed with an equivalent volume of electrophoresis sample buffer containing 10% glycerol (Nacalai Tesque), 2% SDS, 5% 2-mercaptoethanol (Nacalai Tesque) and 0.00125% bromophenol blue (Nacalai Tesque) in 62.5 mM Tris–HCl (pH 6.8). Recombinant bovine Hsc70 protein (SPP-751; Stressgen) and recombinant human Hsp70 protein (NSP-555; Stressgen) were dissolved in the same electrophoresis sample buffer to a concentration of 10 g/ml. All of the samples were heated for 3 min at 100 °C and then cooled to room temperature. A 10 l aliquot of the sample was then loaded onto each lane of Mini-Protean II Ready Gels J (Bio-Rad, Hercules, CA, USA), electrophoresed at a constant voltage of 200 V and then transferred onto polyvinylidene difluoride (PVDF) membranes (Bio-Rad) at a constant voltage of 100 V. After blocking the non-specific reactions with 3% skim milk in 25 mM Tris-buffered saline (TBS), the membranes were incubated with the anti-Hsc70 (SPA-815; 5 g/ml) or anti-Hsp70 antibody (K-20; 2 g/ml) in 25 mM TBS with 3% skim milk for 4 h at room temperature. After washing with 25 mM TBS containing 0.1% Tween-20 (TBST), the membranes were reacted with an alkaline phosphatase-labeled anti-rat IgG (KPL, Gaithersburg, MD, USA, 0.2 g/ml) or anti-goat IgG (Vector, 1:1000) in 25 mM TBS with 3% skim milk for 1 h at room temperature. After rinsing with 25 mM TBST, the primary antibodies were visualized using a 5-bromo-4-chloro-3-indolyl-phosphate/nitroblue tetrazolium (BCIP/NBT) kit (Nacalai Tesque).

Acknowledgments

This work was supported by a grant from the Ministry of Education, Culture, Sports, Science and Technology of Japan, and by a Grant-in-Aid for Scientific Research on Priority Areas from the Ministry of Education, Culture, Sports, Science and Technology of Japan. This work was also supported by a grant from Takeda Medical Research Foundation (Osaka, Japan). The authors thank Hitomi Nakabayashi for her excellent technical assistance.

REFERENCES

Agorogiannis, E.I., Agorogiannis, G.I., Papadimitriou, A., Hadjigeorgiou, G.M., 2004. Protein misfolding in neurodegenerative diseases. Neuropathol. Appl. Neurobiol. 30, 215–224.

Andringa, G., Bol, J.G.J.M., Wang, X., Boekel, A., Bennett, M.C., Chase, T.N., Drukarch, B., 2006. Changed distribution pattern of the constitutive rather than the inducible HSP70 chaperone in neuromelanin-containing neurons of the Parkinsonian midbrain. Neuropathol. Appl. Neurobiol. 32, 157–169.

Auluck, P.K., Chan, H.Y.E., Trojanowski, J.Q., Lee, V.M.-Y., Bonini, N.M., 2002. Chaperone suppression of -synuclein toxicity in a *Drosophila* model for Parkinson's disease. Science 295, 865–868.

Dedmon, M.M., Christodoulou, J., Wilson, M.R., Dobson, C.M., 2005. Heat shock protein 70 inhibits -synuclein fibril formation via preferential binding to prefibrillar species. J. Biol. Chem. 280, 14733–14740.

Dickson, D.W., Liu, W.-K., Hardy, J., Farrer, M., Mehta, N., Uitti, R., Mark, M., Zimmerman, T., Golbe, L., Sage, J., Sima, A., D'Amato, C., Albin, R., Gilman, S., Yen, S.-H., 1999. Widespread alterations of -synuclein in multiple system atrophy. Am. J. Pathol. 155, 1241–1251.

Gai, W.P., Power, J.H.T., Blumbergs, P.C., Blessing, W.W., 1998. Multiple-system atrophy: a new -synuclein disease? Lancet 352, 547–548.

Gilman, S., Low, P.A., Quinn, N., Albanese, A., Ben-Shlomo, Y., Fowler, C.J., Kaufmann, H., Klockgether, T., Lang, A.E., Lantos, P.L., Litvan, I., Mathias, C.J., Oliver, E., Robertson, D., Schatz, I.,

Wenning, G.K., 1999. Consensus statement on the diagnosis of multiple system atrophy. J. Neurol. Sci. 163, 94–98.
Graham, J.G., Oppenheimer, D.R., 1969. Orthostatic hypotension and nicotine sensitivity in a case of multiple system atrophy. J. Neurol. Neurosurg. Psychiatry 32, 28–34.
Jakes, R., Spillantini, M.G., Goedert, M., 1994. Identification of two distinct synucleins from human brain. FEBS Lett. 345, 27–32.
Kato, S., Nakamura, H., Hirano, A., Ito, H., Llena, J.F., Yen, S.-H., 1991. Argyrophilic ubiquitinated cytoplasmic inclusions of Leu-7-positive glial cells in olivopontocerebellar atrophy (multiple system atrophy). Acta Neuropathol. 82, 488–493.
Kawamoto, Y., Akiguchi, I., Nakamura, S., Budka, H., 2002. Accumulation of 14-3-3 proteins in glial cytoplasmic inclusions in multiple system atrophy. Ann. Neurol. 52, 722–731.
Klucken, J., Shin, Y., Masliah, E., Hyman, B.T., McLean, P.J., 2004. Hsp70 reduces -synuclein aggregation and toxicity. J. Biol. Chem. 279, 25497–25502.
Komori, T., Ishizawa, K., Arai, N., Hirose, T., Mizutani, T., Oda, M., 2003. Immunoexpression of 14-3-3 proteins in glial cytoplasmic inclusions of multiple system atrophy. Acta Neuropathol. 106, 66–70.
Krüger, R., Kuhn, W., Müller, T., Woitalla, D., Graeber, M., Kösel, S., Przuntek, H., Epplen, J.T., Schöls, L., Riess, O., 1998. Ala30Pro mutation in the gene encoding -synuclein in Parkinson's disease. Nat. Genet. 18, 106–108.
Lin, W.-L., DeLucia, M.W., Dickson, D.W., 2004. -Synuclein immunoreactivity in neuronal nuclear inclusions and neurites in multiple system atrophy. Neurosci. Lett. 354, 99–102.
Murayama, S., Arima, K., Nakazato, Y., Satoh, J., Oda, M., Inose, T., 1992. Immunocytochemical and ultrastructural studies of neuronal and oligodendroglial cytoplasmic inclusions in multiple system atrophy: 2. Oligodendroglial cytoplasmic inclusions. Acta Neuropathol. 84, 32–38.
Nakazato, Y., Yamazaki, H., Hirato, J., Ishida, Y., Yamaguchi, H., 1990. Oligodendroglial microtubular tangles in olivopontocerebellar atrophy. J. Neuropathol. Exp. Neurol. 49, 521–530.
Ohtsuka, K., Suzuki, T., 2000. Roles of molecular chaperones in the nervous system. Brain Res. Bull. 53, 141–146.
Papp, M.I., Lantos, P.L., 1994. The distribution of oligodendroglial inclusions in multiple system atrophy and its relevance to clinical symptomatology. Brain 117, 235–243.
Papp, M.I., Kahn, J.E., Lantos, P.L., 1989. Glial cytoplasmic inclusions in the CNS of patients with multiple system atrophy (striatonigral degeneration, olivopontocerebellar atrophy and Shy–Drager syndrome). J. Neurol. Sci. 94, 79–100.
Pollanen, M.S., Dickson, D.W., Bergeron, C., 1993. Pathology and biology of the Lewy body. J. Neuropathol. Exp. Neurol. 52, 183–191.
Polymeropoulos, M.H., Lavedan, C., Leroy, E., Ide, S.E., Dehejia, A., Dutra, A., Pike, B., Root, H., Rubenstein, J., Boyer, R., Stenroos, E.S., Chandrasekharappa, S., Athanassiadou, A., Papapetropoulos, T., Johnson, W.G., Lazzarini, A.M., Duvoisin, R.C., Iorio, G.D., Golbe, L.I., Nussbaum, R.L., 1997. Mutation in the -synuclein gene identified in families with Parkinson's disease. Science 276, 2045–2047.
Sharp, F.R., Massa, S.M., Swanson, R.A., 1999. Heat-shock protein protection. Trends Neurosci. 22, 97–99.
Shin, Y., Klucken, J., Patterson, C., Hyman, B.T., McLean, P.J., 2005. The co-chaperone carboxyl terminus of Hsp70-interacting protein (CHIP) mediates -synuclein degradation decisions between proteasomal and lysosomal pathways. J. Biol. Chem. 280, 23727–23734.
Spillantini, M.G., Schmidt, M.L., Lee, V.M.-Y., Trojanowski, J.Q., Jakes, R., Goedert, M., 1997. -Synuclein in Lewy bodies. Nature 388, 839–840.
Tu, P.-h., Galvin, J.E., Baba, M., Giasson, B., Tomita, T., Leight, S., Nakajo, S., Iwatsubo, T., Trojanowski, J.Q., Lee, V.M.-Y., 1998. Glial cytoplasmic inclusions in white matter oligodendrocytes of multiple system atrophy brains contain insoluble -synuclein. Ann. Neurol. 44, 415–422.
Uryu, K., Richter-Landsberg, C., Welch, W., Sun, E., Goldbaum, O., Norris, E.H., Pham, C.-T., Yazawa, I., Hilburger, K., Micsenyi, M., Giasson, B.I., Bonini, N.M., Lee, V.M.-Y., Trojanowski, J.Q., 2006. Convergence of heat shock protein 90 with ubiquitin in filamentous -synuclein inclusions of -synucleinopathies. Am. J. Pathol. 168, 947–961.
Wakabayashi, K., Matsumoto, K., Takayama, K., Yoshimoto, M., Takahashi, H., 1997. NACP, a presynaptic protein, immunoreactivity in Lewy bodies in Parkinson's disease. Neurosci. Lett. 239, 45–48.
Wakabayashi, K., Yoshimoto, M., Tsuji, S., Takahashi, H., 1998a. -Synuclein immunoreactivity in glial cytoplasmic inclusions in multiple system atrophy. Neurosci. Lett. 249, 180–182.
Wakabayashi, K., Hayashi, S., Kakita, A., Yamada, M., Toyoshima, Y., Yoshimoto, M., Takahashi, H., 1998b. Accumulation of -synuclein/NACP is a cytopathological feature common to Lewy body disease and multiple system atrophy. Acta Neuropathol. 96, 445–452.
Wenning, G.K., Ben Shlomo, Y., Magalhães, M., Daniel, S.E., Quinn, N.P., 1994. Clinical features and natural history of multiple system atrophy: an analysis of 100 cases. Brain 117, 835–845.

THE JOURNAL OF BIOLOGICAL CHEMISTRY
Vol. 280, No. 22, Issue of June 3, pp. 21515–21521, 2005
Printed in U.S.A.

Unsaturated Fatty Acids Induce Cytotoxic Aggregate Formation of Amyotrophic Lateral Sclerosis-linked Superoxide Dismutase 1 Mutants*

Received for publication, February 28, 2005
Published, JBC Papers in Press, March 29, 2005, DOI 10.1074/jbc.M502230200

Yeon-Jeong Kim‡, Reiko Nakatomi§, Takumi Akagi§, Tsutomu Hashikawa§, and Ryosuke Takahashi‡¶‖

From the Laboratories for ‡Motor System Neurodegeneration and §Neural Architecture, RIKEN Brain Science Institute, Saitama 351-0198, Japan and ¶Department of Neurology, Kyoto University Graduate School of Medicine, Kyoto 606-8507, Japan

Formation of misfolded protein aggregates is a remarkable hallmark of various neurodegenerative diseases including Alzheimer disease, Parkinson disease, Huntington disease, prion encephalopathies, and amyotrophic lateral sclerosis (ALS). Superoxide dismutase 1 (SOD1) immunoreactive inclusions have been found in the spinal cord of ALS animal models and patients, implicating the close involvement of SOD1 aggregates in ALS pathogenesis. Here we examined the molecular mechanism of aggregate formation of ALS-related SOD1 mutants *in vitro*. We found that long-chain unsaturated fatty acids (FAs) promoted aggregate formation of SOD1 mutants in both dose- and time-dependent manners. Metal-deficient SOD1s, wild-type, and mutants were highly oligomerized compared with holo-SOD1s by incubation in the presence of unsaturated FAs. Oligomerization of SOD1 is closely associated with its structural instability. Heat-treated holo-SOD1 mutants were readily oligomerized by the addition of unsaturated FAs, whereas wild-type SOD1 was not. The monounsaturated FA, oleic acid, directly bound to SOD1 and was characterized by a solid-phase FA binding assay using oleate-Sepharose. The FA binding characteristics were closely correlated with the oligomerization propensity of SOD1 proteins, which indicates that FA binding may change SOD1 conformation in a way that favors the formation of aggregates. High molecular mass aggregates of SOD1 induced by FAs have a granular morphology and show significant cytotoxicity. These findings suggest that SOD1 mutants gain FA binding abilities based on their structural instability and form cytotoxic granular aggregates.

Amyotrophic lateral sclerosis (ALS)[1] is a progressive and fatal neurodegenerative disorder that mainly affects motor neurons in the brain stem and spinal cord. Approximately 10% of ALS patients are familial cases, with autosomal dominant inheritance. More than 90 different mutations in the gene coding for superoxide dismutase 1 (SOD1) have been identified in about 20% of familial ALS (FALS) families (1, 2). Although the molecular mechanisms of selective motor neuron degeneration by SOD1 mutants in FALS remain largely unknown, common pathological features of conformational diseases, as evidenced by SOD1 immunoreactive inclusions, are found in the spinal cord of ALS patients and in the SOD1 mutant FALS mouse model (3–8). The characteristics of FALS resemble those of many other neurodegenerative diseases in which a causative protein undergoes a conformational rearrangement, which endows it with a tendency to aggregate and form deposits within affected tissues.

SOD1 is a 32-kDa homodimeric enzyme that decreases the intracellular concentration of superoxide radicals by catalyzing their dismutation to O_2 and H_2O_2. ALS-linked mutations of SOD1 are distributed throughout the primary and tertiary structures, and most mutations appear unrelated to the dismutase activity. Many biochemical and biophysical studies have reported that SOD1 mutants are structurally unstable compared with wild-type forms (10–13). These observations suggest that the mutations primarily affect the structural stability of SOD1 rather than the enzyme activity.

The half-life of SOD1 mutants is shorter than that of wild-type forms in cultured cells (14). SOD1 mutants form a complex with Hsp70 and CHIP, which promotes degradation of SOD1 through the ubiquitin-proteasome system (15). Hsp70 directly binds metal-deficient wild-type SOD1 as well as SOD1 mutants, suggesting that destabilized SOD1 is targeted by the molecular chaperone system (15, 16). These observations imply that structural stability of SOD1 may also be strongly involved in refolding by the chaperone or in degradation of SOD1 by the ubiquitin-proteasome system. On the other hand, aggregates of mutant SOD1 are observed to have aggresome-like morphology when cells are treated with a proteasome inhibitor (14). This aggresome-like morphology resembles pathological inclusions of neurodegenerative diseases in affected tissues. These findings suggest that in disease states, misfolded proteins overwhelm the protein handling systems, including chaperones and proteasomes. Therefore, the formation of cellular inclusions may be required for other factors to act as modulators to promote protein aggregates. In fact, lipid molecules, including unsaturated fatty acids (FAs), phosphatidylserine, and phosphatidylinositol, promote amyloidogenesis of amyloid β-peptides, tau (17), and α-synuclein (18, 19) *in vitro*. These molecules are biologically significant as mediators for signal-

* This work was supported by research grants from RIKEN Brain Science Institute and a grant-in-aid from the Ministry of Education, Culture, Sports, and Technology of Japan. The costs of publication of this article were defrayed in part by the payment of page charges. This article must therefore be hereby marked "*advertisement*" in accordance with 18 U.S.C. Section 1734 solely to indicate this fact.

‖ To whom correspondence should be addressed: Dept. of Neurology, Kyoto University Graduate School of Medicine, 54 Kawahara-cho, Shogoin, Sakyo-ku, Kyoto 606-8507, Japan. Tel.: 81-75-751-3770; Fax: 81-75-761-9780; E-mail: ryosuket@kuhp.kyoto-u.ac.jp.

[1] The abbreviations used are: ALS, amyotrophic lateral sclerosis; FALS, familial amyotrophic lateral sclerosis; SOD1, superoxide dismutase 1; FA, fatty acid; AA, arachidonic acid; MTS, 3-(4,5-dimethylthiazol-2-yl)-5-(3-carboxymethoxyphenyl)-2-(4-sulfophenyl)-2*H*-tetrazolium.

ing and inflammation during disease progression of neurodegeneration.

Here we investigated *in vitro* SOD1 aggregation affected by FAs to create an aggregation model system for FALS. We demonstrated that unsaturated FAs promote self-assembly and cytotoxic aggregate formation of SOD1. Aggregation by FAs is strongly correlated with structural instability and FA binding activity of SOD1, which may have significant implications in FALS.

EXPERIMENTAL PROCEDURES

Expression, Purification, and Characterization of Recombinant SOD1 Proteins—pcDNA3-SOD1 (20) was digested with EcoRV and XhoI and subcloned into blunted NcoI and XhoI sites of pET-15(b) (Novagen) to construct the expression plasmid. Expression of recombinant SOD1 proteins was induced in BL21(DE3)pLysS by adding 1 mM isopropyl 1-thio-β-D-galactopyranoside, 0.1 mM $CuCl_2$, and 0.1 mM $ZnCl_2$ until cells were grown to 0.6 absorbance unit at 600 nm, and then bacterial cells were further cultured at 23 °C for 6 h. Cells were pelleted and resuspended in TNE buffer (50 mM Tris-HCl, pH 8.0, 150 mM NaCl, and 0.1 mM EDTA) supplemented with protease inhibitor mixture (Roche Applied Science). Cells were then disrupted by sonication. Insoluble materials were removed by centrifugation at 10,000 × *g* for 30 min. Supernatant was collected for further purification. Purification was performed according to Hayward *et al.* (11), with minor modifications. Briefly, ammonium sulfate powder was added to the supernatant to 65% saturation with gentle stirring on ice. The supernatant, after centrifugation at 10,000 × *g* for 30 min, was directly loaded for phenyl-Sepharose (Amersham Biosciences) column chromatography. The column was thoroughly washed with TNE buffer containing 2 M ammonium sulfate. Proteins were eluted using a linearly decreasing salt gradient. SOD1 activity measurement using a xanthine/xanthine oxidase-based method (21) identified fractions containing SOD1. Activity fractions were desalted by ultrafiltration using a centricon filter (Millipore). SOD1 was re-metallated as described previously (22). The proteins were then loaded onto a Q-Sepharose (Amersham Biosciences) anion exchange column and eluted using a linearly increasing salt gradient toward a buffer containing 200 mM NaCl and 10 mM Tris-HCl, pH 8.0. Fractions containing SOD1 were pooled and concentrated. Homogeneity of SOD1 was >95%, as verified by SDS-PAGE with Coomassie Brilliant Blue staining. Specific activity of the purified enzymes was assayed and calculated by bovine SOD1 (Cayman) or human SOD1 purified from erythrocytes (Sigma-Aldrich) as standards. Fully metallated SOD1 was delipidated using hydroxyalkoxypropyl dextran type III (Sigma-Aldrich) as described previously (19) before de-metallation. Metal-deficient apo-enzymes were prepared as described previously (23), and loss of enzyme activity was confirmed after de-metallation. The metal content of purified enzymes was estimated as described previously (22).

Oligomerization of SOD1—A stock solution of 25 mM FAs was prepared in 0.01 M NaOH containing 25 μM butylated hydroxytoluene. SOD1 proteins were filtered through Microcon YM-100 (100-kDa cutoff) filters (Millipore) to remove high molecular mass SOD1 before oligomerization. FAs were added directly to preincubated SOD1 at 37 °C in 50 mM phosphate buffer, pH 7.2, containing 150 mM NaCl and 0.1 mM EDTA and further incubated at the same temperature.

SDS-PAGE and Western Blotting—For detection of SOD1 oligomers, SDS-PAGE was performed under non-reducing conditions using 12.5% polyacrylamide gels. After oligomerization of SOD1, protein samples were prepared in SDS-PAGE loading buffer (62.5 mM Tris-HCl, pH 6.8, 1% SDS, 5% glycerol, and 0.007% bromphenol blue) in the absence of β-mercaptoethanol and then boiled at 95 °C for 3 min before loading. Western blotting was performed as described previously (24). Briefly, proteins were transferred to Hybond ECL nitrocellulose membranes (Amersham Biosciences), followed by UV cross-linking, boiling membranes in 2% SDS and 50 mM Tris, pH 7.6, for 10 min, and extensive washing in Tris-buffered saline. For detection of SOD1, rabbit anti-SOD1 antibody (Stressgen) was used.

Glycerol Density Gradient Centrifugation and Densitometric Analysis—A glycerol linear gradient of 10–40% was prepared in a centrifuge tube. Formation of the SOD1 oligomer was performed as described above. Approximately 200 μl of incubated SOD1 was layered onto a glycerol cushion and separated by centrifugation with a SW41Ti rotor (Beckman) at 35,000 rpm for 15 h. In a parallel experiment, protein standards (Amersham Biosciences) were separated simultaneously in order to calibrate fractions. Fractions were subjected to SDS-PAGE under non-reducing conditions, and then Western blotting was performed. Western blot images were analyzed using image analysis software (Scion Image Beta 4.02; Scion Corp.).

Solid-phase Oleic Acid Binding—Sodium salt of oleic acid (Sigma-Aldrich) was coupled to EAH-Sepharose (Amersham Biosciences) by 1-ethyl-3-(3-dimethylaminopropyl)-carbodiimide (Pierce) to prepare oleate-Sepharose according to Peters *et al.* (25). Oleic acid coupling was verified by binding bovine serum albumin and recombinant α-synuclein protein. Mock-Sepharose was prepared from EAH-Sepharose by blocking coupling ligand with 1 M acetic acid. For the binding assay, 200 ng of Microcon-filtered protein was incubated with oleate-Sepharose or mock-Sepharose in 400 μl of phosphate-buffered saline containing 0.1 mM EDTA at 37 °C for 30 min with agitation. Protein bound to Sepharose was settled on a spun column and washed extensively with phosphate-buffered saline. The bound protein was then eluted with 50% ethanol. Eluates were subjected to SDS-PAGE and Western blotting.

Transmission Electron Microscopy—SOD1 proteins (40 μM) were incubated at 37 °C for 24 h in 50 mM phosphate buffer (pH 7.2) containing 150 mM NaCl and 0.1 mM EDTA supplemented with 100 μM arachidonic acid. The samples were absorbed to a glow-charged supporting membrane on 400-mesh grids and fixed by floating on 2.5% glutaraldehyde and 4% paraformaldehyde in 0.1 M phosphate buffer for 5 min. After three washes with distilled water, samples were negatively stained by 2% sodium phosphotungstic acid and dried. Specimens were observed in a LEO 912AB electron microscope (LEO Electron Microscopy), operated at 100 kV.

Toxicity Assay—Cytotoxicity of protein aggregates was measured as described previously (26, 27). In brief, neuro2a mouse neuroblastoma cells were maintained in Dulbecco's modified Eagle's medium with 10% fetal bovine serum and 2 mM glutamine in 5% CO_2 at 37 °C. Cells were differentiated in serum-free Dulbecco's modified Eagle's medium with 0.3 mM dibutylyl cAMP before use. Cells were plated at 30,000 cells/well in 96-well plates and differentiated overnight. The medium was removed, and prepared SOD1 aggregates were added in new medium without phenol red. After incubation for 18 h at 37 °C, the cells were assayed using an MTS reduction assay kit (Promega). Another plate also treated as described above was stained for 1 min with trypan blue, and stained cells were counted as dead cells.

RESULTS

Unsaturated Fatty Acids Promote Self-assembly of SOD1s—We expressed and homogeneously purified recombinant human SOD1s from the bacterial expression system (Fig. 1*A*). The purified wild-type and G93A enzymes showed comparable specific activity; however, A4V mutant showed ~56% activity compared with that of wild-type enzyme (Fig. 1*B*). The zinc ion content of the purified enzymes showed almost full occupancy; however, copper ion content of A4V was 54.5% of the wild-type level (Fig. 1*C*). Specific activity was correlated with copper ion occupancy of purified enzyme, indicating proper metal loading in the active site.

We next examined the effect of long-chain FAs on oligomerization of SOD1 proteins. Wild-type and mutant (A4V and G93A) SOD1 were incubated with various concentrations of arachidonic acid (AA) as described under "Experimental Procedures." After incubation, oligomerized SOD1 was subjected to SDS-PAGE and then detected by Western blotting. Under reducing conditions, mainly bands of ~16 and 38 kDa, corresponding to monomer and dimmer sizes of SOD1, respectively, were detected (Fig. 2*A*). In contrast, under non-reducing conditions, smeared patterns of >50 kDa in size were supposed to be SOD1 oligomers (Fig. 2*A*). These observations suggest that disulfide bonds maintained SOD1 oligomers. Thus, non-reducing SDS-PAGE was thought to be an efficient method to detect SOD1 oligomers and aggregates. Among the holo-enzymes, wild-type and G93A were not oligomerized; instead, they segregated as monomer and dimer size bands (Fig. 2*B*, *top panel*). After incubation with >100 μM AA, holo-A4V showed a faint smear pattern that was seen from 50 kDa to near the stacking gel range beside monomer- and dimer-size bands (Fig. 2*B*, *top panel*). In contrast, all metal-deficient enzymes, regardless of mutations, were oligomerized in the presence of >30 μM AA

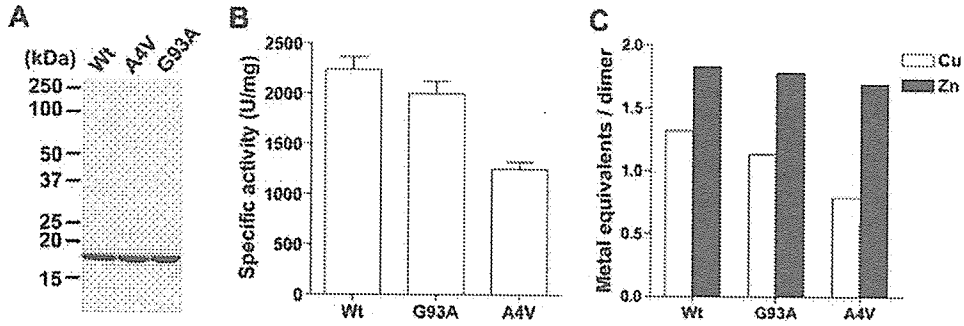

FIG. 1. **Characterization of purified recombinant SOD1s.** *A*, purified SOD1s were separated using SDS-PAGE and stained with Coomassie Brilliant Blue. *B*, dismutase activity of the purified SOD1s was assayed by the xanthine/xanthine oxidase-based method. One unit of the activity is defined as the amount of enzyme needed to exhibit 50% of dismutation of the superoxide radicals. *C*, metal content of the purified SOD1s was measured using 4-pyridylazoresorcinol assay in 6 M guanidine-HCl.

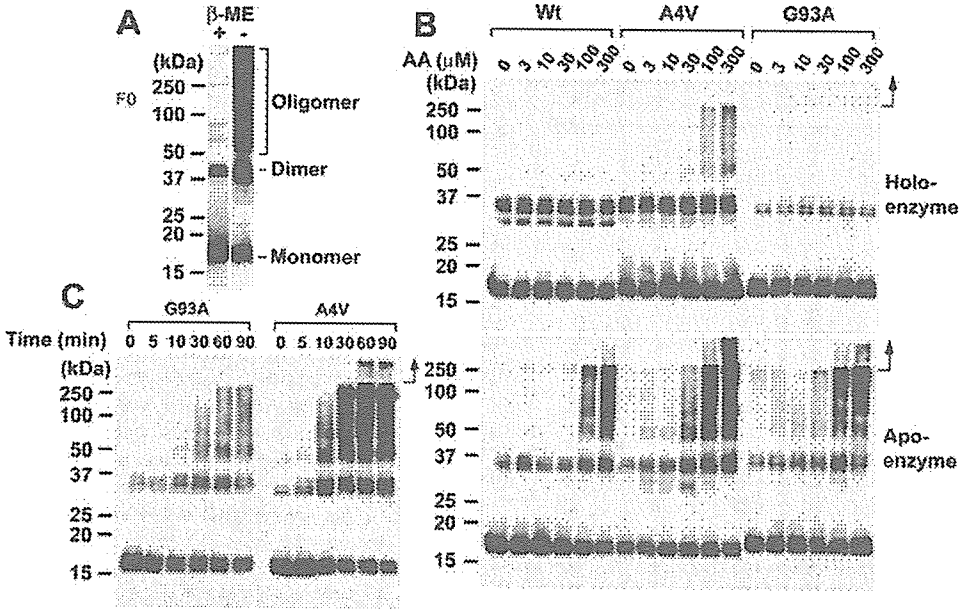

FIG. 2. **Arachidonic acid promotes SOD1 oligomerization.** *A*, FA-inducing oligomers of SOD1 were separated using SDS-PAGE with or without β-mercaptoethanol. *B*, apo-enzymes of SOD1 mutants (2.5 μM) were incubated at 37 °C in the presence of 100 μM AA. At each time point, aliquots were placed on ice to stop the reaction. *C*, purified holo- or apo-SOD1 proteins (2.5 μM) were incubated at 37 °C for 90 min in the presence of the indicated AA concentration. Incubated proteins were mixed directly with SDS-PAGE treatment buffer without reducing agents and boiled. SDS-PAGE was performed under non-reducing conditions. Proteins were detected by Western blotting as described under "Experimental Procedures." *Arrows* indicate the position of stacking gels.

(Fig. 2*B*, *bottom panel*). Apo-enzymes demonstrated higher oligomerization propensity than holo-enzymes depending on AA concentration (Fig. 2*B*). Thus, AA efficiently promoted oligomerization of SOD1s.

Next, we performed a time-course analysis of SOD1 oligomerization in the presence of AA. Metal-deficient G93A and A4V were oligomerized in a time-dependent manner (Fig. 2*C*). Maximum oligomerization was reached within 60 min of incubation in the presence of AA (Fig. 2*C*).

We then examined the effect that various FAs, including stearic acid, oleic acid, linoleic acid, and AA, have on SOD1 oligomerization. Unsaturated FAs, including oleic acid, linoleic acid, and AA, promoted SOD1 oligomerization (Fig. 3). However, saturated FAs and stearic acid had little effect on SOD1 oligomerization (Fig. 3). SOD1 oligomerization induced by FAs required at least monounsaturated FAs. This result may reflect the difference of solubility between unsaturated and saturated FAs in the buffer.

We verified the formation of SOD1 oligomers using a 10–40% glycerol density gradient centrifugation because presumable artifacts after detection of SOD1 oligomers using non-reducing SDS-PAGE may have remained. After fractionation, we could not observe high molecular mass SOD1 oligomers

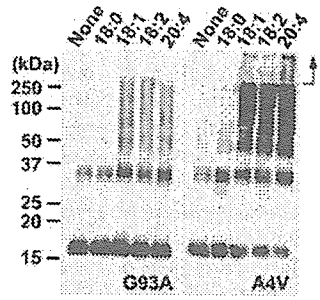

FIG. 3. **Unsaturated fatty acids affect oligomerization of SOD1.** Apo-enzymes of SOD1 mutants were incubated at 37 °C for 90 min in the presence of FAs at concentrations of 100 μM: 18:0, stearic acid; 18:1, oleic acid; 18:2, linoleic acid; and 20:4, arachidonic acid. *Arrows* indicate the position of stacking gels.

from the incubated sample in the absence of AA; fractions were <67 kDa and potentially represented monomer and dimer states (Fig. 4*A*, *top panel*). In contrast, we detected high molecular mass oligomers in fractions of >440 kDa from the incubated sample in the presence of AA (Fig. 4*A*, *bottom panel*). Under these conditions, SOD1 with molecular mass of <67 kDa was dramatically decreased compared with the sample incu-

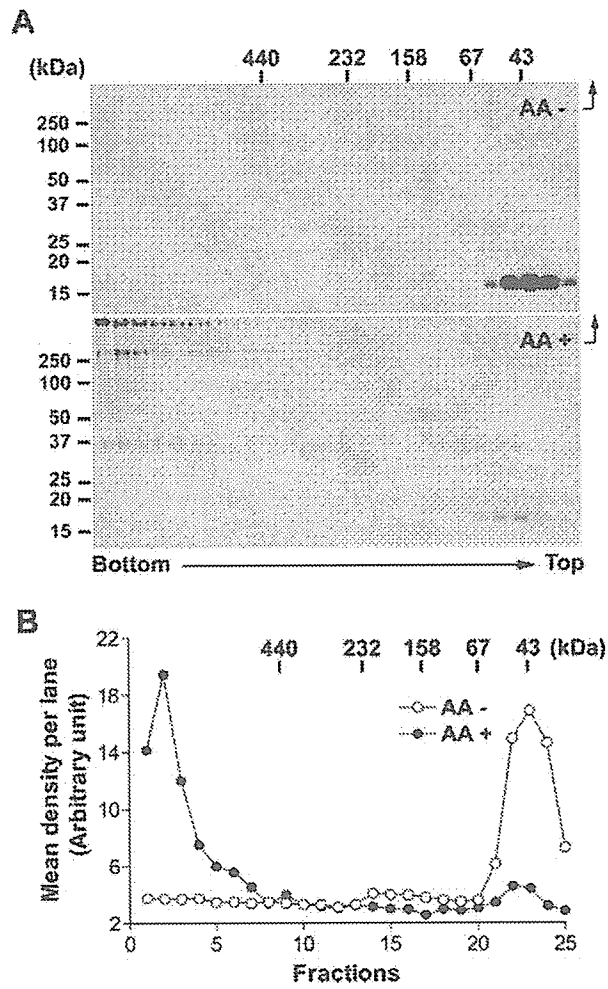

FIG. 4. **Glycerol density gradient centrifugation and densitometric analysis of SOD1 oligomers.** *A*, apo-A4V (2.5 μM) was incubated at 37 °C for 90 min in the absence or presence of 100 μM AA before loading on the glycerol cushion. After centrifugation, fractions were collected from the bottom of the tubes and then subjected to SDS-PAGE under non-reducing conditions. SOD1 proteins were detected by Western blotting. *B*, for densitometric analysis, we measured mean density per lane after background subtraction. Total mean density was similar under each condition, by calculating the mean density of visible lanes (*lanes 1–8* for oligomers and *lanes 21–25* for dimer or monomer). *Arrows* indicate the position of stacking gels.

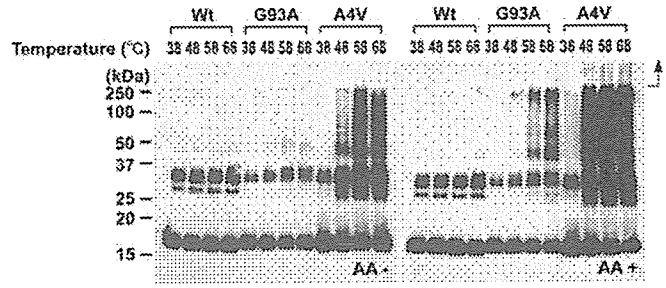

FIG. 5. **Thermally destabilized SOD1 mutants show a high oligomerization propensity.** Holo-enzymes were heat-treated at the indicated temperatures for 30 min before addition of 100 μM AA and then further incubated at 37 °C for 1 h. SDS-PAGE was performed under non-reducing conditions. Proteins were detected by Western blotting as described under "Experimental Procedures." *Arrows* indicate the position of stacking gels.

bated in the absence of AA (Fig. 4*A*, *bottom panel*). Although oligomers of >440 kDa were fractionated by the glycerol density gradient centrifugation, these were detected as monomer, dimer, and smeared high molecular mass bands that reached stacking gels under non-reducing SDS-PAGE (Fig. 4*A*, *bottom panel*). This indicates oligomers are partly disrupted during the boiling of the SDS-PAGE loading buffer. We next performed densitometric analysis from Western blotting images to estimate the amount of oligomerized SOD1 (Fig. 4*B*). The resulting image analysis found that immunoreactivity for oligomers was ~80% of the total immunoreactivity.

Structural Instability of SOD1 Is Correlated to Oligomerization Propensity and FA Binding—We showed the FA-induced oligomerization propensity of apo-SOD1s was higher than that of holo-SOD1. This implies that protein stability might be strongly associated with FA-induced oligomerization propensity. Among the holo-enzymes, wild-type and G93A were not oligomerized under our experimental conditions (Fig. 2*B*, *top panel*). To examine the correlation between oligomerization propensity and protein stability of holo-enzymes, holo-SOD1 was heated and then oligomerized by AA. In the absence of AA, only heat-treated A4V was oligomerized (Fig. 5, *left panel*). In the presence of AA, heat-treated G93A and A4V were highly aggregated, but under the same conditions, wild-type SOD1 was not (Fig. 5, *right panel*). Oligomerization was observed above 58 °C for G93A and above 48 °C for A4V (Fig. 5, *right panel*). In the previous study, A4V was more unstable than G93A for heat treatment analyzed by differential scanning calorimetry (12). This result suggests that structural instability is strongly correlated with oligomerization propensity induced by FAs.

Although we showed that FAs promoted SOD1 oligomerization, the mechanism is not perfectly understood. Similarly, unsaturated FAs oligomerize α-synuclein and tau. In the case of α-synuclein and tau, FAs were bound to proteins, which suggested that oligomerization mechanisms underlie the FA binding characteristics of protein. To examine whether SOD1 binds to FAs, we carried out a solid-phase oleic acid binding assay. Among the holo-enzymes, very small amounts of holo-A4V were bound to the oleate-Sepharose column, whereas wild-type and G93A were not (Fig. 6*A*). All of the apo-enzymes were bound to oleate-Sepharose, regardless of their mutations (Fig. 6*A*). In contrast, bound proteins were not observed in mock-Sepharose (Fig. 6*A*). Nearly all of the input amounts of metal-deficient proteins were bound, which was estimated by 50% input. This finding suggests that metal-deficient SOD1 proteins strongly bind to FAs. We next examined whether heat-treated holo-enzymes bind to FAs. Apo-enzymes were used as control binding. Heat-treated SOD1 mutant (G93A) at 58 °C and 68 °C was bound to FAs, whereas wild-type was not (Fig. 6*B*). The results of the FA binding assay were strongly correlated with the oligomerization propensity of SOD1. These findings suggest that FA binding alters the conformation of SOD1 to form oligomers.

FA-induced SOD1 Aggregates Result in Granular Morphology and Are Cytotoxic—We analyzed the ultrastructure of SOD1 aggregates by electron microscope. SOD1 proteins (~40 μM) were incubated in the presence of 100 μM AA at 37 °C for 24 h. Holo-enzymes were heated at 50 °C for 30 min before incubation in the presence of AA. After incubation, granular aggregates were observed in all of apo-enzymes and heat-treated SOD1 mutants (Fig. 7*A*). In contrast, no visible materials were found in wild-type holo-SOD1s, even though they were heat-treated (Fig. 7*A*). The morphology of the aggregates was round or amorphous large granules composed of clustered small granules (Fig. 7*A*). We could not observe any visible protein aggregates in the samples incubated without AA, except in apo-A4V, which revealed a fibril structure (data not shown).

We next examined the effect of FA-induced aggregates on cell

viability of differentiated neuro2a cells. Aggregates of SOD1s were formed using the same methods as described for observation under an electron microscope. Aliquots incubated in the presence or absence of AA were diluted in the culture medium, which was directly added to differentiated neuro2a cells. After incubation for 18 h, toxicity was assessed with MTS reduction (Fig. 7*B*) and trypan blue staining (Fig. 7*C*). The presence of the granular aggregates formed by AA from Apo-SOD1s and heat-treated SOD1 mutants significantly reduced cell viability (Fig. 7, *B* and *C*). In contrast, no significant decrease of viability was detected when the cells were exposed either to incubated proteins in the absence of AA or to the buffer solutions used to form the aggregates in the absence of added protein (Fig. 7, *B* and *C*). These findings suggest that FA-induced SOD1 aggregates were highly toxic to the cells.

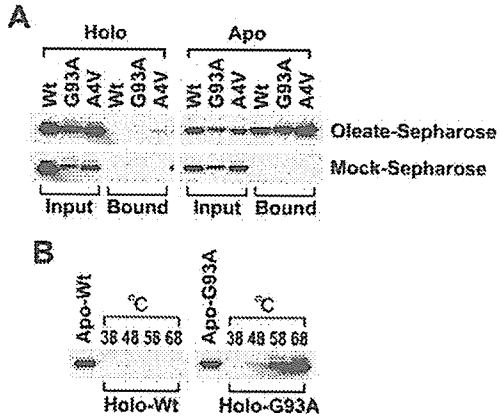

FIG. 6. **Solid-phase oleic acid binding assay shows apo-SOD1 or thermally destabilized SOD1 bound to oleate-Sepharose.** *A*, solid-phase binding assay was performed as described under "Experimental Procedures." Approximately 50% input (100 ng of proteins) was electrophoresed to estimate the quantity of FA binding SOD1. *B*, holo-SOD1s (wild-type and G93A) were thermally destabilized at the indicated temperatures for 30 min and then directly loaded on oleate-Sepharose. Apo-enzymes were used as positive controls for oleic acid binding.

DISCUSSION

Numerous neurodegenerative diseases are accompanied by highly insoluble inclusions of protein aggregates within characteristic neuronal populations. In the case of FALS, the protypical Lewy body-like hyaline inclusions, composed largely of granule-coated fibrils of SOD1-insoluble filaments, have been detected in the spinal cord of FALS patients with SOD1 gene mutations (5, 28). Although there has been controversy about whether such inclusions are a cause or a consequence of the neuronal degeneration, accumulating evidence suggests that aggregates formed via misfolded proteins, especially soluble oligomeric assemblies, may cause cell injury (29–31). Moreover, cytotoxicity of protein aggregates may have common features because granular aggregates form non-pathological proteins that can also be toxic (26). These findings suggest the avoidance of protein aggregation may be crucial for therapy of

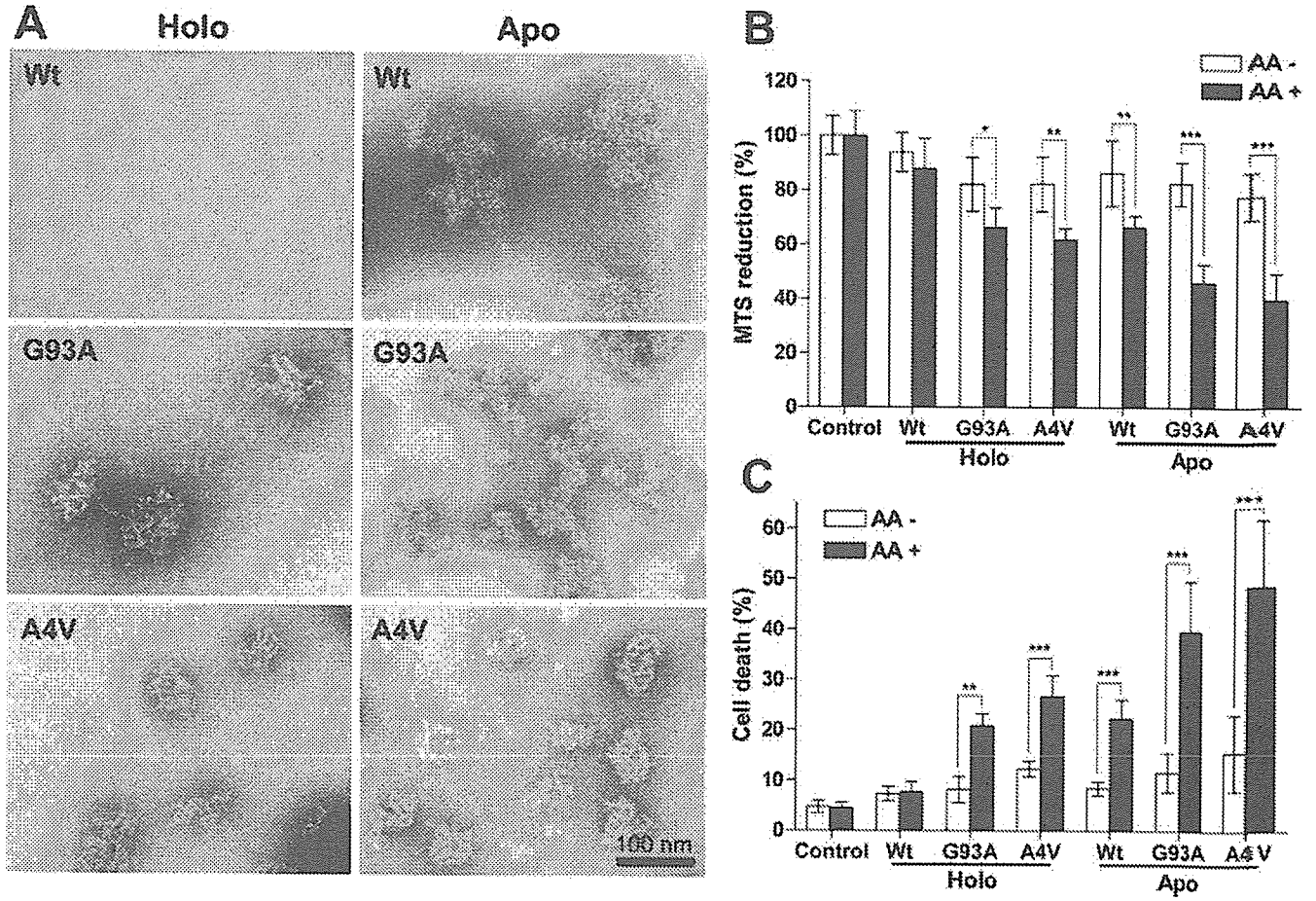

FIG. 7. **SOD1 aggregates and their cytotoxicity for the differentiated neuro2a cells.** Holo-SOD1s were pre-heated at 50 °C for 30 min before incubation with AA. SOD1 proteins (40 μM) were incubated in the presence of 100 μM AA at 37 °C for 24 h before observation under an electron microscope (*A*). Differentiated neuro2a cells were directly exposed for 18 h in medium containing incubated aliquots of SOD1s with or without arachidonic acid. The concentration of SOD1 in the culture medium was 4 μM. Buffer and AA carryover in the culture medium was controlled. Cytotoxicity was assessed using an MTS reduction assay (*B*) and trypan blue exclusion staining (*C*). The results were analyzed by two-way analysis of variance. The values are the means ± S.D. (n = 6). *, $p < 0.05$; **, $p < 0.01$; ***, $p < 0.001$.